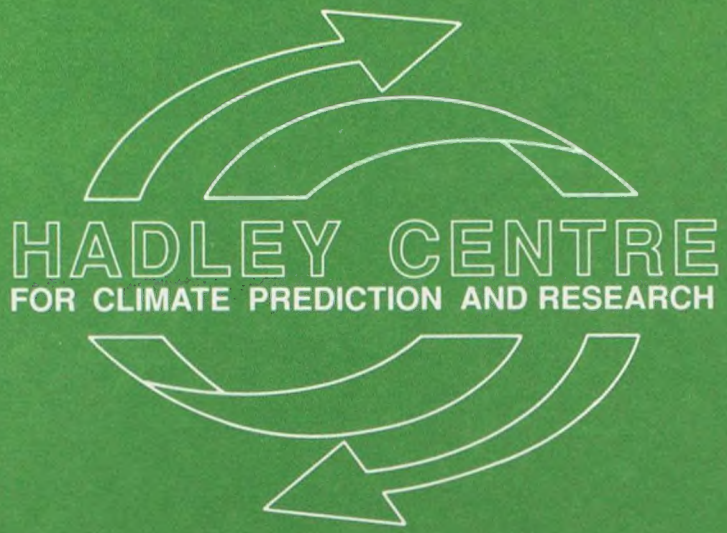

Use of wind stresses from operational N.W.P. models to force an O.G.C.M. of the Indian Ocean

by

D. J. Carrington

CRTN 10 **April 1991**

CLIMATE
RESEARCH
TECHNICAL
NOTE

Hadley Centre
Meteorological Office
London Road
Bracknell
Berkshire RG12 2SY

CLIMATE RESEARCH TECHNICAL NOTE NO. 10

USE OF WIND STRESSES FROM OPERATIONAL N.W.P. MODELS TO FORCE AN O.G.C.M. OF THE INDIAN OCEAN

by

D J CARRINGTON

Hadley Centre for Climate Prediction and Research
Meteorological Office
London Road
Bracknell
Berkshire RG12 2SY
U.K.

NOTE: This paper has not been published. Permission to quote from it should be obtained from the Director of the Hadley Centre.

ABSTRACT

Wind stresses taken from the operational NWP models of the UK Met Office (MO) and the European Centre for Medium range Weather Forecasts (EC) have been used to force an Ocean General Circulation Model of the Indian Ocean. With both MO and EC stresses the major features of the Indian Ocean upper level circulation are simulated. Significant interannual variability is produced in response to the NWP stresses, but the variability in current strengths produced by the two different NWP models' fields can be nearly as great as the interannual variability. Validation of the model simulations by comparison of the model Dynamic Height with Geosat altimetry data has been attempted and it yields generally encouraging results.

1. Introduction

In the early 1980's, the World Climate Research Program of the World Meteorological Organisation inaugurated an international coordinated program of research, called TOGA (Tropical Oceans Global Atmosphere) to run from 1985 to 1995. It is designed to investigate the interactions between the tropical oceans and the atmosphere with a view to furthering the understanding of this coupled system and ultimately to forecast its changes (WCRP, 1985)

TOGA consists of two main streams of research: observational and modelling. The principal aim of the modelling program is to produce a realistic fully coupled operational model of the tropical oceans and global atmosphere. The achievement of this objective is necessarily a step-by-step process: each of the tropical oceans is studied separately, and a hierarchy of models is used to explore the physical processes involved.

One of the contributions being made to this research by the Meteorological Office Unit at the Hooke Institute in Oxford is the development of an Ocean General Circulation Model (OGCM) of the Indian Ocean for hindcasting the upper-level circulation. In a previous paper (Carrington, 1990) a description of the model was given and an assessment made of its ability to simulate the climatological currents in the Indian Ocean in response to climatological forcing. In this paper the next step in developing the hindcasting capability of the model is discussed, namely the use of wind stresses derived from operational Numerical Weather Prediction (NWP) model analyses to force the model. In a subsequent paper the use of heat fluxes from NWP models to force the ocean model will be presented.

The use of forcing fields from NWP models enables two questions to be addressed. Firstly, how much interannual variability is there in the Indian Ocean circulation? The seasonal cycle of currents in the Indian Ocean is fairly well known, but there are insufficient observational data for estimates to be made of the amount of interannual variability except in one or two limited areas such as the Somali Current region. A model forced with the best available estimates of the actual forcing fields therefore provides a tool with which to study the interannual variability. Some studies have been carried out using NWP model data to force simple ocean models, but this is the most extensive study so far performed with an Ocean General Circulation Model.

Secondly, how much variability in the ocean model simulations is produced as a function of the particular NWP model from which the forcing fields are taken?

By implication, therefore, what does this indicate regarding both the sensitivity of the ocean model to external forcing and the relative accuracy of the different NWP model fields?

The model simulations of the circulation produced in response to forcing by NWP wind stresses inevitably contain errors with respect to the true circulation. There are two causes of these errors - weaknesses in the ocean model and errors in the forcing fields - and it is not possible to separate their relative contributions entirely. Observations, particularly of currents, with which to validate the model simulations are sparse, and it is therefore difficult to make reliable quantitative statements from the model simulations about the magnitude of interannual variability or to draw firm conclusions about which NWP model fields are "better". Nevertheless, the model simulations enable a preliminary impression to be made of the ocean variability and qualitative conclusions to be drawn.

2. Experiments performed

The details of the model are described in a previous paper (Carrington, 1990). In brief, it is a "primitive equation" model (the so-called "Cox model" after Cox, 1984) with a domain from 27°N to 36°S and from 35°E to 118.5°E; the resolution is variable, with a minimim grid-spacing on the Equator near the western boundary of 1/2° x 1/3° and a maximum of 1½° x 1°; there are 16 levels in the vertical, and the barotropic mode is excluded from the solution. Two experiments were carried out in which wind stresses taken from the analyses of operational NWP models were used to force the model.

Wind stresses were taken from the NWP model analyses of the Meteorological Office (MO) and the European Centre for Medium-range Weather Forecasts (EC). With the MO data, 6-hourly fields were averaged over periods of 3 days. With the EC data, 6-hourly fields were used to create monthly means; these were then linearly interpolated to form values at 3-day intervals. The MO forecast model analysis data was on a 1.5°x1.875° latitude-longitude grid and the EC data on a 1.125°x1.125° grid; these were interpolated onto the Indian Ocean model grid.

MO data were obtained for the period November 1986 to May 1990, and the ocean model has been integrated using the data for this period. EC data have been obtained for the period August 1985 to December 1988. In order to make the experiments with the two NWP model fields as directly comparable as possible, integration with the EC stresses was begun with data for November 1986 and continued until December 1988.

Stresses are now a standard diagnostic of both atmospheric forecast models and are derived using the boundary layer scheme incorporated in the models. The Met. Office stresses up to May 1987, however, had to be separately calculated from the 10m wind field; this was done using a constant drag coefficient of 1.0×10^{-3}.

The initial conditions for the experiments were taken from the seasonal cycle experiment (described in the previous paper) which had been spun up for three years using the climatological wind stress forcing of Hellerman & Rosenstein (1983) from the climatological temperature and salinity fields of Levitus (1982).

The heat and salinity fluxes used in both experiments were the same as in the seasonal cycle experiment; the heat fluxes were based on the climatology of Esbensen & Kushnir (1981) with a negative (Haney) feedback to climatological sea surface temperature (using the SST climatology of Bottomley et al, 1989), and

the salinity fluxes derived from the precipitation and evaporation climatologies of Jaegar (1976) and Esbensen & Kushnir respectively with a negative feedback to the climatological surface salinity of Levitus. The heat and salinity flux schemes are described in more detail in the previous paper.

3. Interannual variability (using MO stresses)

In order to study the interannual variability produced by the model in response to wind stresses taken from NWP models, the experiment in which MO stresses were used will be examined. Though the period for which the model has been integrated (November 1986 to May 1990, namely 3½ years) is too short to provide any meaningful statistical evaluation of interannual variability, it is long enough for qualitative statements to be made.

The years 1987 and 1988 will be compared in most detail for two reasons. Firstly, the strength and timing of the Southwest Monsoon was very different in the two years, and so 1987 and 1988 provide a good example of the magnitude of interannual variability which can occur. Secondly, these are the only two years for which the corresponding wind stresses from the European Centre NWP model have been obtained and so this is the period used also for comparing the results obtained from the two different forcing fields in Section 4. The currents in 1989 and early 1990 will be cited in less detail.

3.1 Surface Currents

a) The Southwest Monsoon period (May to Sept.)

The period of the Southwest Monsoon and its onset and demise provides the most significant interannual variability in the currents. The 1987 Southwest Monsoon is recognized as having been very weak; most areas of India received between 20% and 50% less rainfall than the average (Das et al, 1988). By contrast the 1988 Monsoon produced above average rainfall over much of India (Das et al, 1989). Fig.3.1 shows the mean monthly wind stress from the MO forecast model for July 1987 and July 1988; in 1987 the maximum stress in the Arabian Sea was about 2.5 dynes/cm^2, but in 1988 it was 4 dynes/cm^2. The different ocean model currents reflect this difference in winds between the years. Fig.3.2 shows the currents for April, May and June 1987; Fig.3.3 shows the equivalent currents for 1988; Fig.3.4 shows the difference between the currents in May in the two years (May 1988 minus May 1987).

The magnitudes of the simulated currents in 1988 are very similar to those simulated by the model when forced by climatological wind stresses; the only major difference is in the equatorial currents simulated during the latter part of the SW Monsoon, which will be discussed in subsection 3.3. below. This is in

contrast with those in 1987, especially during the onset phase of the SW Monsoon.

i) The Wyrtki Jet

This eastward current on the Equator developed only weakly in Apr-Jun 1987, having a speed of only 20cm/s in May and reaching 40cm/s in the western equatorial region in June (Fig.3.2c). This compares with speeds in excess of 100cm/s across the central equatorial region by May in 1988 (Figs.3.3b & 3.4). In May 1989 it was also strong (over 80cm/s) and in May 1990 slightly weaker (50cm/s). The Wyrtki Jet following the end of the summer monsoon, however, shows much greater consistency in strength; its maximum strength in November in all years 1986 to 1989 was over 80cm/s.

ii) Reversal in the cross equatorial flow (CEF)

Th reversal of the cross equatorial flow along the western boundary was slower and later in 1987 than in 1988. In 1988 a southward flow of 30cm/s in April (Fig.3.3a) changed to a northward flow of 80cm/s in May (Fig.3.3b); this is similar to climatology. In 1987 there was scarcely any cross-equatorial flow in May at all (Figs.3.2b & 3.4), though in June the velocity reached over 80cm/s northwards (Fig.3.2c). In 1989 the southward flow in April was similar to that in 1988, but the northward flow in May was weaker (50cm/s). In 1990 the flow was already slack by April, but the May current was similar to that in 1988.

iii) Somali Current

This was of similar strength in June 1987 and June 1988, with a maximum of just over 100cm/s over a small region. In July and August 1987, this region remained small, migrating northwards up the coast. In the same months in 1988, by contrast, an extensive region with currents greater than 120cm/s developed. With the demise of the Southwest Monsoon and the spinning down of the Somali Current, the current strengths in September and October were similar in the two years. In 1989 the strength of the Somali Current was similar to that in 1988, though the region of currents greater than 100cm/s extended slightly less far north in July and August.

iv) The Southwest Monsoon Current (SMC)

This eastward flow north of the Equator, around southern India and Sri Lanka, was stronger and developed earlier in 1988, when it reached a peak of over 120cm/s in June (Fig.3.3c), persisting at 60cm/s through July and August. In

1987 the June maximum was only about 60cm/s (Fig.3.2c); in July and August it persisted at a 60cm/s maximum as in 1988 but this time with a stronger (50cm/s) anticyclonic recirculating gyre in the Bay of Bengal. In 1989 the SMC was of similar strength to that in 1988.

b) The Northeast Monsoon period (Nov. to March)

The differences between the years in the currents during the NE monsoon period show a less consistent pattern through the season than was the case for the SW Monsoon; some months show significant differences, others do not. The strengths of the equatorial currents in November are similar in 1987 and 1988, as mentioned above. In December, however, the eastward current on the Equator has a maximum of over 100cm/s in 1987 but little over 40cm/s in both 1986 and 1988; in 1989 there is westward flow over much of the equatorial region, with a maximum of over 40cm/s. By January, in contrast, the currents are very similar in 1988 and 1990 (40-60cm/s westward). The southward Cross Equatorial Flow is stronger in November 1987 than in November 1988 (a maximum of over 20cm/s in 1987 compared with little more than 10cm/s in 1988), but the December CEF is stronger in 1988 (in excess of 60cm/s compared with about 50cm/s in 1987).

The magnitude of the interannual variability of these features is therefore large. In the equatorial regions differences in maximum current speeds are commonly 30-50cm/s and can be as large as 100cm/s. This reflects the rapid speed with which equatorial currents can be generated in response to the applied wind stress. For the principal off-equatorial currents (notably those along the western boundary and the Southwest Monsoon Current) the magnitude of interannual variability is less but can be as great as 50cm/s.

3.2 Sub-surface currents

Interannual variability is also seen in the equatorial sub-surface currents. Fig.3.5 shows a depth-time plot of zonal velocity at 73°E on the Equator. The strength of the eastward EUC, towards the end of the NE Monsoon, for example, peaks at greater than 60cm/s at 73°E in 1987 (and also in 1989) but is less than 40cm/s in 1988, whilst the eastward surface current following it is considerably stronger in 1988. A consistent pattern is seen at other points on the Equator (not shown). A large degree of interannual variability has been

observed in the EUC at this time of year in previous years (Knox, 1976; McPhaden, 1982). Similar, though less marked, variability in the strength of the EUC at other times of the year is also apparent from Fig.3.5.

Also visible in Fig.3.5 is a positive slope in the depth of the velocity maxima and minima as a function of time. This upward propagation in the phase of the velocity variation is associated with downward propagation of Rossby waves from the surface layers (Luyten & Roemmich, 1982; Gill, 1982).

3.3 Equatorial currents during the latter part of the SW Monsoon (July to Sept.)

The need to be able to validate the model simulations is highlighted by the surprising nature of the simulated equatorial currents during the latter part of the Southwest Monsoon.

The surface currents produced in the 1988 simulation are, as mentioned above, generally very similar over much of the year to those produced in the experiment in which climatological wind stresses were used (the results of which are in good agreement with climatological currents). However, the simulated equatorial currents during the latter part of the SW Monsoon for 1988 are significantly different to climatological currents; moreover, they are similar in 1987 and 1988, in spite of the fact that, in other respects, the currents for these two years are very different. A strong westward current, which dominates the equatorial region, is produced in both years, the eastward SMC being restricted to the region immediately around the Indian subcontinent. Fig.3.6a & b show the currents for August 1987 and July 1988, which were the months when the strength of the westward current peaked in 1987 and 1988 respectively, and Fig.3.6c shows the currents for July 1989, when the westward current is a relatively minor feature and strong eastward flow dominates the eastern equatorial region; the July simulation from the climatological experiment is given in Fig.3.7.

The rapid speed at which equatorial currents can be spun up by a zonal component of wind has been discussed in Carrington (1990). The contrast between the currents of July 1989 and those of the previous years may be explained by the difference in the applied wind stress. Fig.3.8 shows the wind stress fields from the MO forecast model for July 1989; refer back to Fig.3.1 for the equivalent fields for July 1987 and July 1988. It may be seen that in 1989 the SE Trades in the eastern equatorial region turn SW before crossing the Equator,

thus producing a westerly component of wind stress on the Equator; in 1988, by contrast, the Trades remain southeasterly until after crossing the Equator, and an easterly component of wind stress on the Equator is produced. The currents generated by the model illustrate the sensitivity of the ocean model to equatorial stresses. Differences in the zonal wind stress as small as 0.2-0.3 dynes/cm^2 can give rise to differences in currents as high as 100-150cm/s.

It is not possible to confirm whether or not the strong simulated westward currents are realistic. The differences between the NWP model and climatologically-forced runs may be so large because the Hellerman & Rosenstein stresses are inaccurate, because the zonal component of the Met. Office stresses is too high, or because extremely large interannual variability does exist. Some climatologies of surface currents (e.g. Hastenrath, 1985) include no westward current on the Equator during this period. Others, however, (e.g. Cutler & Swallow, 1984) show a weak (10-20cm/s) westward current. Measurements made by Knox (Knox, 1976) show that a westward current at least as strong as 70cm/s can occur for short periods (see Fig.3.9), though this observed current was evidently not a simple response to local equatorial easterlies since these were negligible at the time. Whether the strong simulated westward current is realistic will be discussed further in Sections 4 and 5.

3.4 Summary

Some of the features of interannual variability produced when the model is forced by wind stresses taken from the MO NWP model analyses have been examined, and the need for validation of the simulations is apparent. This may be attempted either by using external data sources or by using forcing fields from another NWP model. This latter approach results in variability in the simulations as a function of the NWP model fields used, and it will be discussed first.

4. Use of different NWP model stresses (MO and EC)

The Indian Ocean model has been integrated using stresses obtained from the European Centre (EC) operational NWP model analyses. The period for which comparable integrations have been carried out using both MO and EC wind stresses extends from November 1986 to December 1988 and therefore includes the 1987 and 1988 Monsoon seasons.

For the purpose of this section, the experiment in which MO wind stresses were used will be referred to as EXPMO and that in which EC stresses were used as EXPEC. The currents simulated in EXPEC will be compared to those obtained in EXPMO, with emphasis being given to the same circulation features discussed in Section 3.

4.1 Surface currents

To simplify comparison of the equatorial currents in EXPEC and EXPMO, time-versus-longitude plots of monthly-mean zonal velocity at 5m depth on the Equator for EXPMO and EXPEC are presented in Fig.4.1a & b, with the difference field (EXPMO minus EXPEC) in Fig.4.1c.

a) Southwest Monsoon (May to Sept.)

i) Wyrtki Jet

In EXPEC the Wyrtki Jet preceeding the Southwest Monsoon is, as in EXPMO, stronger in 1988 than in 1987 but to less marked a degree: greater than 100cm/s in 1988 and over 60cm/s in 1987 (compared with over 100cm/s and over 40cm/s respectively in EXPMO). The maxima occur further east - by 15° in 1989 and 10° in 1988. As in EXPMO, the maximum occurs in June in 1987 and in May in 1988 (Fig.4.1).

The Wyrtki Jet in November shows greater variability in EXPEC than in EXPMO. Maximum currents are less than 60cm/s in 1987 and over 80cm/s in 1988 (compared with over 80cm/s in both years in EXPMO).

ii) Somali Current

The general features of the Somali Current are very similar in the two simulations, and in both cases the maximum velocities generated are a little over 100cm/s. However, the current turns away from the coast to form the "Great

Whirl" slightly further south in EXPEC than in EXPMO (by 1-2°), and the double-gyre structure (with a second circulation to the south of the Great Whirl) which has been observed to develop in most years (Swallow & Fieux, 1982) but is not well reproduced in EXPMO is better simulated in EXPEC (Figs.4.2 & 3.6b). This is highlighted in Fig.4.3 which shows the difference in 5m currents between EXPEC and EXPMO for July 1988.

There is less difference in the strength of the Somali Current between 1987 and 1988 in EXPEC than in EXPMO. The region with currents greater than 100cm/s in July and August is fairly extensive in both 1987 and 1988 in EXPEC (this region was very small in 1987 in EXPMO - see Figs.4.4 & 3.6a). The region is less elongated parallel to the coast but extends further offshore, which is consistent with the general circulation features described above.

iii) Cross Equatorial Flow

At the times of reversal in direction of the CEF, there are significant differences between the two simulations. In particular, the CEF changes to flowing northward earlier in EXPEC than in EXPMO in both 1987 and 1988: in May 1987 there is a northward flow of over 20cm/s (compared with a slack or weak southward flow in EXPMO see Figs.4.5 & 3.2b), and in April 1988 there is a northward flow of 5cm/s (compared with over 30cm/s southward). The strength of the northward flow slackens later in EXPEC; in August 1988 the flow is over 80cm/s (compared with over 40cm/s in EXPMO).

During the rest of the year, including during the Southwest Monsoon itself, the strength of the flow is very similar in the two simulations.

iv) Southwest Monsoon Current

The peak strength of the SMC is similar in EXPEC and in EXPMO. However, in both years it spins down significantly earlier in EXPEC: in September 1987 it has a maximum of 40cm/s (compared with over 60cm/s in EXPMO), and in October 1988 its maximum is 10cm/s (compared with over 60cm/s). In 1987, it also builds later in EXPEC: in June 1987 it has a maximum of over 30cm/s (compared with over 60cm/s in EXPMO).

v) Westward Equatorial currents

The westward equatorial currents which were generated in the latter part of the Southwest Monsoon in EXPMO are present in EXPEC too, but they are not as strong. In 1987 the maximum velocity is just over 20cm/s (compared with over 60cm/s in EXPMO); the difference in strength is in excess of 40cm/s over a

large region (Fig.4.1c). In 1988 the maximum velocity in EXPEC is over 60cm/s (compared with over 100cm/s in EXPMO); the transition from the eastward Wyrtki Jet to the westward current occurs later, such that in June and July 1988 there is a large difference between the simulations (Fig.4.1c).

This raises the possibility that the strong westward currents produced using MO stresses may partly be explained by inaccuracies in the wind stress field. Further mention is made of this, however, in Section 4.3 below.

b) Northeast Monsoon period

In the November equatorial currents there is greater difference between 1987 and 1988 than in EXPMO (see section on Wyrtki Jet above). In the December currents there is less difference between the years, however (Fig.4.1); a maximum in the eastward current of about 40cm/s is produced in both 1987 (compared with over 100cm/s in EXPMO) and 1988 (similar to that in EXPMO).

4.2 Subsurface currents

The pattern of subsurface currents in EXPMO and EXPEC is similar. A depth-time plot of zonal velocity at 73°E on the Equator is presented in Fig.4.6 and can be compared with Fig.3.5. In general the maxima in the currents occur at a slightly shallower depth in EXPEC (by about 20-50m), and below 200-250m the currents in EXPEC are weaker. Though the strengths of the currents differ between the two experiments, there is no consistent pattern as to which experiment has the stronger currents.

4.3 Summary and discussion

The Indian Ocean model simulates the significant seasonal circulation features of the Indian Ocean in response to both MO and EC wind stresses. The difference in the strength of the Southwest Monsoon between 1987 and 1988 is reflected in the surface currents in both cases. There are, however, significant differences between the simulations, both of a random nature and of a more systematic type.

The systematic differences are most evident in the equatorial region and along the Somali coast. Along the Equator, the EC zonal wind stresses have a greater eastward component, especially in the eastern half of the Indian Ocean; Fig.4.7 shows time-versus-longitude plots of monthly-mean zonal wind stress on

the Equator for EXPMO and EXPEC and the difference field (EXPMO minus EXPEC). Because of the speed with which zonal equatorial currents can be spun up, the larger eastward component in the EC wind stress results in a greater eastward component in the surface currents in EXPEC than in EXPMO. This is the case throughout the year. In particular, the westward currents produced on the Equator during the latter part of the Southwest Monsoon using MO stresses are considerably weaker (and more similar to climatology) when EC stresses are used. The question remains open, however, as to whether this is because the MO stresses are less accurate or because the EC NWP analyses are more strongly biased towards a climatology which has a relatively strong eastward component in climatological wind stress in this data-sparse region.

The equatorial currents generated by MO stresses generally also exhibit a greater range of strength than those generated by EC stresses; in most cases the equatorial currents generated by MO stresses, whether eastward such as the Wyrtki Jet or westward, are stronger than those generated by EC stresses, though this is not universally the case.

There are differences between the simulations of the Somali Current region. With EC stresses the current turns offshore further south (by 1-2°) and a stronger gyre structure and recirculation is produced. Other systematic differences include the timing of the reversals in the Cross Equatorial Flow and the spinning down of the Southwest Monsoon Current.

In Section 3, the magnitude of the interannual variability produced using MO stresses was described, the differences being greatest in the regions of strongest currents during the Southwest Monsoon. The magnitude of the variability produced as a result of the two NWP forcing fields is often of a similar magnitude. Differences in the range 30-50cm/s are not infrequent and on occasion are as great as 80cm/s (for example on the Equator in June 1988). Outside the period of the Southwest Monsoon, the differences are much smaller and the simulations generally agree well (the main exception being the equatorial currents in the eastern part of the Ocean).

In two cases there is observational evidence that one simulation consistently reproduces a particular circulation feature more realistically than the other. Thus, the latitude at which the Somali Current turns offshore and the strength of the recirculation simulated with EC stresses is in closer agreement with observations (e.g. Swallow et al, 1983). Further, the strength of the westward currents on the Equator towards the end of the Southwest Monsoon with MO stresses appears unreasonably large. But with regard to most features, it is not possible to conclude which simulation is the more realistic without external

validation of the surface currents in that particular month.

Attempts to provide external validation will be considered in the next section.

5. External validation

5.1 Available methods

Observational data coverage of the world's oceans on a routine basis is notoriously poor and most surface-based observations are restricted to the principal shipping routes. The advent of the capability of satellites to measure ocean surface properties (especially sea surface temperature and height) has, in recent years, begun to increase the observational data-base.

For validation of the ocean model simulations for which wind stresses taken from operational NWP model analyses were used, the ideal data to use would be direct measurements of the surface currents. If these are not available, then some indirect measure of the flow regime or thermal structure would provide at least an estimate of the accuracy of the model. Because the surface thermal forcing of the ocean model was strongly biased towards climatology in the experiments, the surface or near-surface temperature field does not provide a useful gauge for validation; this means that satellite and/or ship estimates of sea surface temperature (data which are more readily available on the required space- and time-scales) cannot be used.

There are two principal methods of measurement of surface currents in the open ocean that are employed: the use of moored and floating buoys, and estimation from ship drift. Unfortunately, for the period for which the Indian Ocean model has been integrated using NWP stresses, there have been no buoys in the Indian Ocean. Ship drift data have been used extensively for the derivation of climatologies of surface currents (for example the ship drift data for the Indian Ocean produced by Cutler & Swallow, 1984), but the quantity of data on a month by month basis is insufficient, in the Indian Ocean at least, for validation of the ocean model. (Analysis of the available data in order to explore its potential for model validation will be described in a separate note.)

Only indirect methods of validation are possible, therefore. Two particular sources of data are appropriate: firstly, X.B.T.s (eXpendable BathyThermographs) which measure vertical temperature profiles at specific points; and, secondly, satellite altimetry, which measures sea-surface height and can therefore effectively be used as a measure of the vertically-integrated thermal structure on a basin-wide scale. The use of altimetry data has clear spatial advantages, and to date this is the only method of the two that has been applied to validation of the Indian Ocean model.

The use of altimetry data for model validation involves the comparison of satellite estimates of surface elevation with the fields of Dynamic Height (DH) computed from the model. DH is the component of the sea-level variation which results from changes in the integrated density of the water column beneath the surface. DH is not an automatic diagnostic of the model since the model is constrained to have a rigid lid at its upper boundary. Evaluation of the model DH therefore requires integration over depth of the density structure; Appendix A provides details of how this was done. The satellite estimates of surface elevation are derived from measurements from the Geosat altimeter. The altimeter measurements need to be corrected for variations in the Earth's geoid and atmospheric water vapour to determine the sea-level height, and the effects of tides and variations in atmospheric pressure must be allowed for. The measurements of surface elevation include variations due to the changes in the vertically integrated mass. The model solutions do not contain the barotropic component of the flow, and so the Geosat fields contain an element of variation that the model DH does not; on a monthly mean basis this is unlikely to contribute a significant amount to the variation, however. Appendix B contains background to the use of satellite altimetry for the validation of ocean models.

Cheney et al (1988) and Cheney (private communication) have processed Geosat data for the Indian Ocean from June 1985 onwards to produce monthly sea-level anomaly maps, and from January 1989 onwards the data were processed in near-real-time and published in NMC's Climate Diagnostics Bulletin. These are probably the best estimates available of Indian Ocean DH. Unfortunately during October 1989 there was an instrument malfunction aboard Geosat and altimetry data have not been subsequently available for the Indian Ocean. The maps for November 1986 to September 1989 have been used for validation of the model integrations, both EXPMO and EXPEC.

5.2 Model validation using Dynamic Height

Cheney et al (1988) present the DH anomalies relative to the mean for the year Aug. 1987 - July 1988. For direct comparison the DH of the model simulations is therefore presented in the same manner. A three-way comparison is made here: model simulations from EXPMO and from EXPEC, and Geosat.

a) Seasonal cycle

Before proceeding to a discussion of the experiments in which NWP model

stresses were used, some points can usefully be made regarding the comparison of the model DH from the seasonal cycle experiment (in which climatological wind stresses as well as heat fluxes were used and which is discussed in Carrington, 1990) with observations. The model simulations are consistent with published estimates of the seasonal variation in DH. Agreement is very good, for example, with fields presented by Wyrtki (1971) derived from ship-borne measurements of the thermal structure, though the magnitude of maxima and minima in DH is sometimes exaggerated in the model by the order of 5 dyn cm. Comparison with DH fields calculated from the Levitus temperature and salinity data shows somewhat greater differences in the magnitude of the maxima and minima, of the order of 10 to 15 dyn cm, especially in the Somali region and Arabian Sea.

b) Case study: two sample months

The seasonal cycle is still the dominant signal in both the model simulations with NWP wind stress and the Geosat charts, but there is also some interannual variability. The model and altimetry charts are compared here initially for two months, November 1987 and July 1988; these months illustrate the features typical of the similarities and differences between model and altimeter and between the two model experiments. Figs.5.1 and 5.2 show the simulations from EXPMO and EXPEC and the altimetry measurements for the two months respectively. Fig 5.3 shows the 5m currents from EXPMO for November 1987 to enable cross-referencing of DH and current features to be made; the EXPMO currents for July 1988 may be seen in Fig.3.5b.

On a month-by-month basis, there is reasonable qualitative agreement between model and Geosat; the large-scale features are fairly well-represented by the model. In November 1987, for example, the following features can be seen in all three charts (Fig.5.1): a major trough extending from the equatorial African coast, through the southern Arabian Sea (associated with a cyclonic circulation, with the November Wyrtki Jet on the southern flank) and into the Bay of Bengal (similarly associated with a cyclonic circulation); a ridge extending westwards along the Equator from Indonesia (associated with the eastward flow on the Equator and the subsequent depression of the thermocline in the east); a ridge north of Madagascar (with the westward-flowing South Equatorial Current on its southern side); and a ridge-trough-ridge feature extending east-southeast in the Southern Hemisphere. On the quantitative level, there are significant differences, however. In EXPEC the magnitude of peaks and troughs are generally smaller than in EXPMO. In some cases they underestimate the measurements from Geosat when EXPMO provides a closer estimate (for

example, the trough in the southern Arabian Sea in November 1987 and the ridges both north and south of the Equator in the western region in July 1988). In other cases, it seems to be the more moderate estimates of EXPEC that are closer to Geosat and the magnitudes in EXPMO seem too extreme (for example, the trough in the eastern equatorial region in July 1988, associated with the westward flow on the Equator). Overall the magnitude of peaks and troughs are slightly better represented in EXPMO, but EXPEC appears to resolve better some of the ridge-trough features in the southern Hemisphere (for example, the general structure in the Southern Hemisphere in November 1987).

The two most obvious differences between the model simulations and Geosat are, firstly, the resolution of smaller-scale features in the Southern Hemisphere in Geosat, and, secondly, the representation of the Somali region during the Southwest Monsoon. The first of these is apparent from the noticeably smoother fields in the model simulations of the Southern Hemisphere in both months illustrated. This is likely to be largely because there are very few atmospheric observations in this region and so the NWP models are unable to simulate synoptic-scale features of the circulation; this will then be reflected by the ocean model when forced by wind stress fields obtained from the NWP models. The same was found to be true for the Southern Hemisphere Pacific Ocean when the simulation of DH from the model of Leetmaa & Ji (1988) was compared with Geosat measurements (Miller & Cheney, 1990).

The second of the two major differences, the representation of the Somali region, is more likely to be due to errors in the Geosat charts. The data have been averaged over 2°x1° rectangles, and this will tend to smooth out very small scale features. The "high" in the model DH is associated with the Somali gyre which is anticyclonic amd spins up during the Southwest Monsoon. It is well documented from observations, and a "high" in DH would be expected here.

c) Interannual variability

Though these comparisons between Model and Geosat appear good at first sight, this is largely because of the dominance of the seasonal cycle in the signal. When the interannual variability is examined the agreement is less marked. Fig.5.4 shows the DH fields from EXPMO, EXPEC and Geosat for November 1988 and can be compared with Fig.5.1; Fig 5.5 shows the 5m currents from EXPMO for November 1988. Comparison of Figs.5.1 and 5.5 shows some common features of interannual variability between the model and Geosat fields. For example, the trough extending east-southeast in the eastern part of the Southern Hemisphere which is stronger in 1988 than in 1987 in Geosat is reflected in both model

simulations and is consistent with the stronger currents along the Indonesian coast in 1988; likewise the trough in the southern Arabian Sea is stronger in 1987 which is consistent with stronger equatorial currents on the Equator to the south of this. Other differences apparent in the Geosat charts are not, however, reflected in the model simulations. These two months are fairly typical of the degree of agreement between model and Geosat. When all the months examined are considered, neither EXPMO nor EXPEC simulates the interannual variability noticeably more accurately than the other.

d) Discussion

The interannual variability in the model simulations of DH is likely to be restricted by the climatological thermal forcing used in the experiments. The interannual variability which the NWP wind stresses would tend to produce will therefore be partially "damped" by the thermal forcing. The identical thermal forcing probably also explains the otherwise surprisingly high degree of agreement between the DH from EXPMO and EXPEC given the magnitude of the differences in simulated surface currents described in Section 4. A temperature error of 1°C or a salinity error of 0.3‰ throughout the whole of the mixed layer would produce a DH error of about 2.5cm.

In spite of the relatively weak representation of interannual variability in the model DH, the Geosat DH charts appear to be able also to provide some direct qualitative validation of the model currents. By way of illustration, the Equatorial westward currents simulated by the model during the latter part of the Southwest Monsoon and discussed in previous sections will be considered. The Geosat DH for July 1988 is seen in Fig.5.2c, and the chart for July 1989 is given in Fig.5.6. The longitudinal slope in DH is downward to the west in the former (and is similar to this in August 1987, not shown) but nearer horizontal in the latter. Since a westward equatorial current will tend to result in a depression of the thermocline in the west, this interannual difference in Geosat DH is consistent with a westward current in July 1988 and August 1987 but a more eastward flow in July 1989.

There are numerous factors which probably contribute to the differences between model and Geosat DH fields, some of which have already been discussed. They will be summarised below.

1) Forcing fields

- the difficulty of NWP models accurately to represent synoptic-scale

features in data-sparse regions such as the Southern Hemisphere Indian Ocean is reflected in the wind stress fields and hence in the DH;

- more generally, random and systematic errors in the NWP wind stress fields produce errors in DH. In off-equatorial regions the DH is particularly a function of the curl of the applied wind stress, since this leads to upwelling or downwelling and vertical displacement of the thermocline; since a derivative quantity (the curl) is used, the errors in wind stress are magnified. Leetmaa (1987) and Harrison et al (1989) have emphasised the detrimental effect on model simulations of inaccuracies in the curl of the wind stress;
- use of climatological thermal forcing will tend to reduce interannual variability in DH.

2) Model weaknesses

- surface DH is, to a first order, a measure of the thermocline depth, and the model is probably unable to resolve the thermocline sufficiently accurately. Higher resolution at thermocline depth (for example the resolution attained in the 27-level Pacific model of Philander used by Leetma & Ji, 1988) does produce a sharper thermocline and hence a more accurate simulation of the vertically integrated density structure. This problem is accenuated by the tendency of the model to reduce the sharpness of the thermocline over the course of an extended integration; the model was "spun up" for three years prior to NWP forcing being used, and in this time the thermocline sharpness will have degraded. Morliere et al (1989) highlight the beneficial effect that assimilation of subsurface thermal data has on retaining a sharp thermocline;
- the model is not perfect, and other weaknesses in the model will impact on the simulated DH.

3) Geosat fields

- the process of averaging the fields over 2°x1° rectangles may have the effect of smoothing out the Somali Gyre to some extent;
- the general pre-processing of the Geosat data probably leads to inaccuracies in the DH fields produced;
- the model DH fields are monthly averages whereas the Geosat data are not. The latter are derived from bimonthly measurements and are only a sample of the field at some point during the month; the time for which these derived quantities are truly valid is not constant across the ocean

domain.

- the Geosat fields are of sea surface height, which includes a component due to the barotropic flow. This may make a difference of the order of a few dynamic cm in instantaneous surface height measurements.

5.3 Summary

Comparison of the model DH fields with altimetry data yields generally encouraging results on a qualitative level, indicating that the model does reasonably well at simulating the actual fields in response to forcing by both MO and EC wind stresses. However, there are significant quantitative differences. Many features of interannual variability evident in the altimetry data appear in the model simulations but they are generally only relatively weakly represented; the degree of interannual variability in the model simulations of DH, and the difference between MO and EC simulations, is less than that which might have been anticipated given the high degree of interannual variability in the surface currents. The discrepancies are likely to be due to a combination of errors in the NWP wind stress fields, the use of climatological thermal forcing, model weaknesses and inaccuracies in the Geosat DH charts.

Unfortunately, DH can only be used as an indirect method of validating the model simulations. No method is available for ascertaining whether or not the strengths of the simulated currents are correct.

6. Conclusions

Wind stresses taken from the operational NWP models of the UK Met Office and the European Centre have been used to force an Ocean General Circulation Model of the Indian Ocean.

With both MO and EC stresses the major features of the Indian Ocean upper level circulation are simulated.

Significant interannual variability is produced in response to NWP stresses. In the regions of the strongest currents (the Equatorial region and along the western boundary) the magnitude of this variability can be of a similar order of magnitude to the strength of the currents themselves. Differences between years of 30-50cm/s are common and can be as great as 100cm/s. The variability is greatest during the Southwest Monsoon. The largest differences seen over the period for which the model was integrated are between the Monsoons of 1987 and 1988.

The variability in current strengths produced as a result of fields from the two different NWP model can be nearly as great as the interannual variability. Once again the differences are most acute during the Southwest Monsoon. Some systematic differences are directly attributable to systematic differences in the applied wind stress fields.

Validation of the model simulations by using external data is very difficult. Comparison of model Dynamic Height with Geosat altimetry data yields encouraging results on a qualitative level, but there are significant quantitative differences. There are unfortunately no direct current observations available. It is therefore not possible to make authoritative statements about the magnitude of the interannual variability on the basis of the model simulations, nor to conclude which of the MO or EC stresses produce the more accurate simulation.

The thermal structure of the upper model levels was constrained in the experiments to be close to climatology. It is therefore desirable to use a heat flux scheme which would simulate more accurately the actual thermal structure and, in particular, the SSTs (which govern the effect of the ocean on the atmosphere). Attempts to use heat fluxes derived from NWP model analyses instead of climatological ones to force the model are described in a subsequent paper.

The magnitude of the variability produced by the different NWP model fields indicates the sensitivity of the ocean model to errors in the forcing fields.

One method of reducing the impact of these errors is to assimilate observations (from XBTs or from satellites) into the model. This is to be attempted shortly and, it is hoped, will increase the accuracy of the model simulations.

Appendix A: Model Dynamic Height

Water density is a function of temperature, salinity and pressure. Therefore the integrated volume of a water column depends upon the temperature and salinity at all levels. The height of the ocean surface with respect to some reference level is thus an indicator of the temperature/salinity structure in an integral sense; this is the "dynamic height" (DH), which is analogous to the thickness of the atmosphere between two pressure surfaces. Though the surface temperature and salinity in the model are strongly influenced by climatology, the integrated density with depth can provide at least a "first-order" check on the validity of model results.

The changes in horizontal pressure gradients associated with horizontal variations in density cause, in the presence of the Coriolis force, changes in the geostrophic currents. In the upper levels the Ekman velocity provides an additional velocity component. However, the relative geostrophic component is still dependent upon the density gradient, and at the surface itself this implies a correlation between the gradient of DH and the actual velocity. The gradient of DH of the model ocean is thus an indirect check of the surface currents as well as of the temperature-salinity structure in the model.

The equation of state of ocean water can be approximated such that water density (ρ) may be calculated using a complex polynomial function of temperature, salinity and pressure. Gill (1982) describes how this equation is used. It is conventional to calculate a "standard" DH of the ocean surface for a column of water at 0°C and 35‰; what is loosely described as the DH is then in fact the anomaly relative to this standard. The calculation is made with respect to an assumed level of negligible motion in the ocean.

The model used has a rigid lid and so the T/S structure causes an imputed pressure on the inside surface of the lid instead of a surface displacement. However, what the DH would be if there were a free surface may be calculated from the T/S structure. In order to calculate DH in the model ocean, it is assumed that the temperature and salinity at a grid-point are representative of the whole of the grid-box at which the point is at the centre. The value of ρ for the grid-box is then compared with the "standard", and the contribution of the box to the anomaly in DH can be calculated; the total DH anomaly is the sum over depth of the individual box contributions. The reference level chosen in this study was the grid-point at 798m (i.e. it is assumed that the horizontal

pressure gradient at this level is zero); experiments show that increasing this depth has negligible effect on the results.

Appendix B: Satellite altimetry

Fu et al (1988) provide a useful summary of the methodology of measuring the height of the sea surface by remote-sensing methods and the problems involved. The two-way travel time of a radar pulse is measured, which must be corrected for atmospheric refraction, bias caused by greater scattering in wave troughs, and atmospheric-pressure variations. Comparison of Geosat data with tide-gauge measurements show that the altimetry data are accurate to about 4cm (Cheney et al, 1989). Successive orbits of the satellite cross the Equator 164km apart.

The first detailed ocean-wide analysis of DH was made by Wyrtki (1974) for the Pacific; he used all available oceanographic station data to produce a map of average DH. There are insufficient observations, however, to use this data source for individual months. Satellite measurements of altimetry can provide the required coverage in time and space, and the required data are now becoming available for qualitative assessments at least.

DH measurements have been widely used for comparison purposes, especially in modelling of the Pacific. At NMC, the DH field output from their operational hindcasting model of the tropical Pacific (Leetma & Ji, 1988) is validated routinely against Geosat altimetry data; the model compares favourably with the observations. Leetma & Ji (1990) have also used DH as a diagnostic of the 1986-87 El Niño; they describe the annual cycle of DH in the Pacific and the principal features of interannual variability in that period. Cheney et al (1989) discuss the applicability of altimetry data to Pacific modelling; they point out that in an operational model in which the heat flux scheme keeps the temperature in the upper levels close to the climatological values, interannual variability of the model DH will mainly be caused only by variations in the depth of the thermocline rather than by variations in the density structure of the surface layers as well. This point should also be considered with regard to the MO model of the Indian Ocean.

No detailed comparisons have yet been made between altimetry data and tide-gauge measurements in the Indian Ocean. Delecluse et al (1988) have found a very good level of agreement, however, between Geosat data and the DH simulated using a shallow-water model of the Indian Ocean.

REFERENCES

Bottomley M, Folland CK, Hsuing J, Newel E & Parker DE (1989). "Global Ocean Surface Temperature Atlas (GOSTA)". A joint project of the Meteorological Office and Dept. of Earth, Atmospheric and Planetary Sciences, MIT. In press.

Carrington DJ (1990). An ocean general circulation model of the Indian Ocean for hindcasting studies. Meteorological Office Climate Research Technical Note No. 2 (October 1990).

Cheney RE, Miller L & Doyle NS (1988). Indian Ocean sea level anomaly maps from GEOSAT. (Abstract) EOS Trans. AGU 69(44), 1280.

Cheney RE, Douglas BC & Miller L (1989). Evaluation of Geosat altimeter data with application to tropical Pacific sea level variability. J.Geophys.Res. 94C 4737-4747.

Cutler AN & Swallow JC (1984). Surface currents of the Indian Ocean (to 25°S,100°E): compiled from historical data archived by the Meteorological Office, Bracknell, UK. I.O.S., Wormley, UK, Report No. 187.

Das SN, Rao MRM & Biswas NC (1988). Weather: Monsoon Season (June-September 1987). Mausam 39 325-340.

Das SN, Desai DS & Biswas NC (1989). Weather: Monsoon Season (June-September 1988). Mausam 40 351-364.

Delecluse P, Perigaud C & Fu L-L (1988). Seasonal variations of the dynamic topography in the Indian Ocean from the Geosat altimeter compared to shallow-water simulations (abstract). EOS 69(44) 1267.

Esbensen SK & Kushnir Y (1981). The heat budget of the global ocean: An atlas based on estimates from surface marine observations. Report No.29, Climate Research Institute, Oregon State University, Corvallis.

Fu L, Chelton DB & Zlotnicki V (1988). Satellite altimetry: observing ocean variability from space. Oceanography 1 4-11.

Gill A (1982). "Atmosphere-ocean dynamics". Academic Press.

Haney RL (1971). Surface thermal boundary conditions for ocean models. J.Phys.Ocean. 1 241-248.

Harrison DE, Kessler WS & Giese BS (1989). Ocean circulation model hindcasts of the 1982-83 El Niño: thermal variability along the ship-of-opportunity tracks. J.Phys.Ocean. 19 397-418.

Hastenrath S (1985). Ocean circulation. In "Climate and circulation of the tropics". Reidel.

Hellerman S & Rosenstein M (1983). Normal monthly wind stress over the world ocean with error estimates. J.Phys.Ocean. 13 1093-1104.

Jaegar L (1976). Monthly maps of precipitation for the whole world ocean. D.Wetterd., Ber.18, Nr.139, Offenbach.

Knox RA (1976). On a long series of measurements of Indian Ocean equatorial currents near Addu Atoll. Deep Sea Res. 23 211-221.

Leetma A (1987). Progress towards an operational ocean model of the tropical Pacific at NMC/CAC. In "Further progress in equatorial oceanography". Ed. EJ Katz & JM Witte. Nova Univ. Press, Dania FL.

Leetma A & Ji M (1988). Operational hindcasting of the tropical Pacific. Dyn.Atmos.Oceans 13 465-490.

Leetma A & Ji M (1990). Variability of surface dynamic height in the tropical Pacific during 1985-1987. Submitted to Dyn.Atmos.Oceans.

Levitus S (1982). Climatological atlas of the world ocean. NOAA Prof.Paper No.13.

Luyten JR & Roemmich DH (1982). Equatorial currents at semi-annual period in the Indian Ocean. J.Phys.Ocean. 12 406-413.

McPhaden M (1982). Variability in the central Indian Ocean. Part I: Ocean dynamics. J.Mar.Res 40 157-176.

Miller L & Cheney R (1990). Large-scale meridional transport in the tropical Pacific Ocean during the 1986-87 El Nino from Geosat. J.Geophys.Res (in press).

Morlière A, Reverdin G & Merle J (1989). Assimilation of temperature profiles in a General Circulation Model of the Tropical Atlantic. J.Phys.Ocean. 19 1892-1899.

Swallow JC & Fieux M (1982). Historical evidence for two gyres in the Somali Current. J.Mar.Res. 40 (supplement) 747-755.

Swallow JC, Molinari RL, Bruce JG, Brown OB & Evans RH (1983). Development of near-surface flow pattern and water mass distribution in the Somali Basin in response to the southwest monsoon of 1979. J.Phys.Ocean. 13 1398-1415.

WCRP (1985). Scientific plan for the tropical ocean and global atmosphere programme. WCRP publications series No.3, September 1985. WMO/TD No.64.

Wyrtki K (1971). Oceanographic Atlas of the International Indian Ocean Expedition. Washington: NSF.

Wyrtki K (1974). The dynamic topograpjy of the Indian Ocean and its fluctuations. Hawaii Institute of Geophys., Report HIG-74-5.

Fig.3.1 Mean-monthly wind-stress (dynes/cm²) from the Met. Office global forecast model analyses for (a) July 1987 and (b) July 1988.

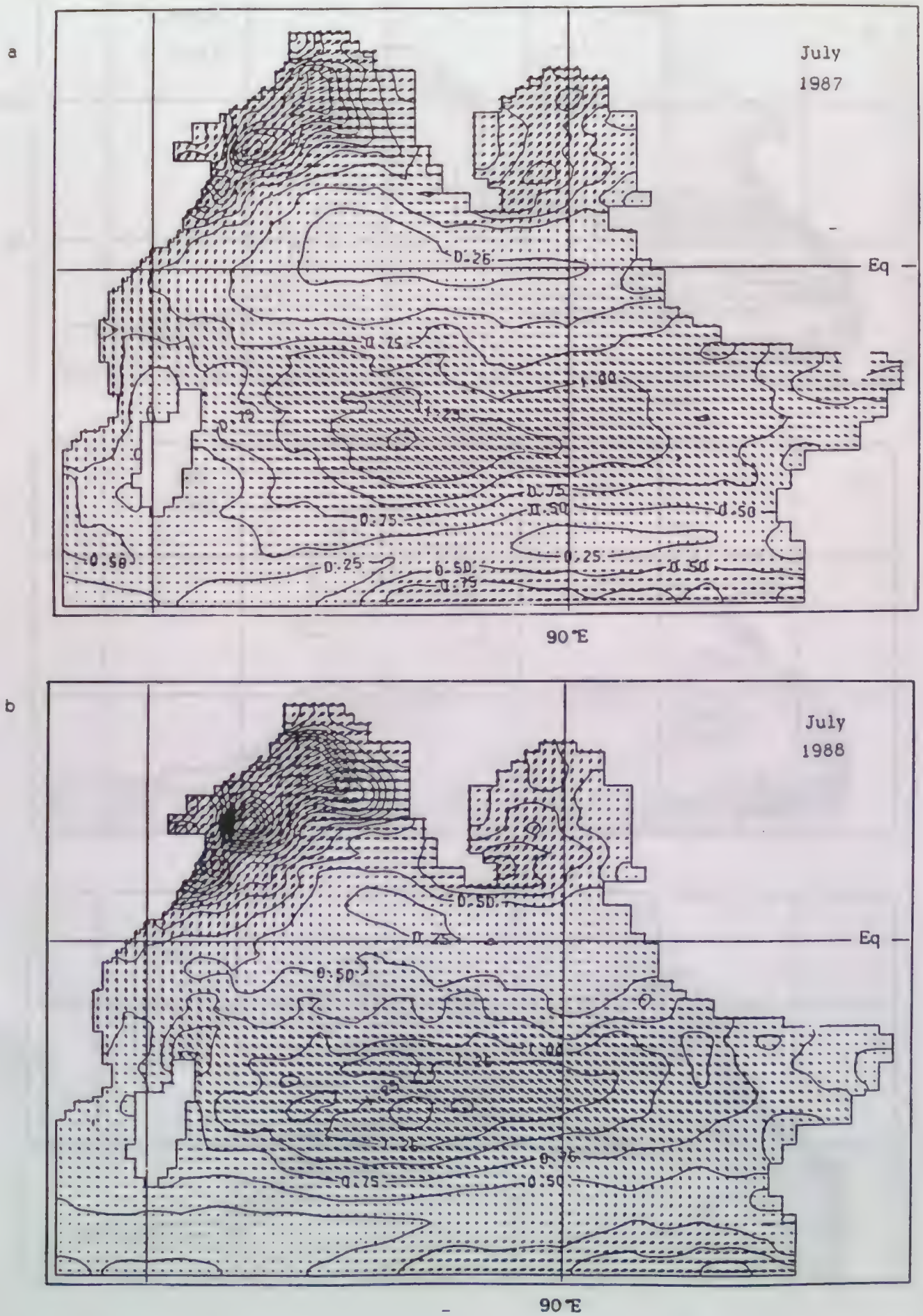

Fig.3.2 Experiment using MO stresses: 5m currents (cm/s) for (a) April, (b) May and (c) June 1987.

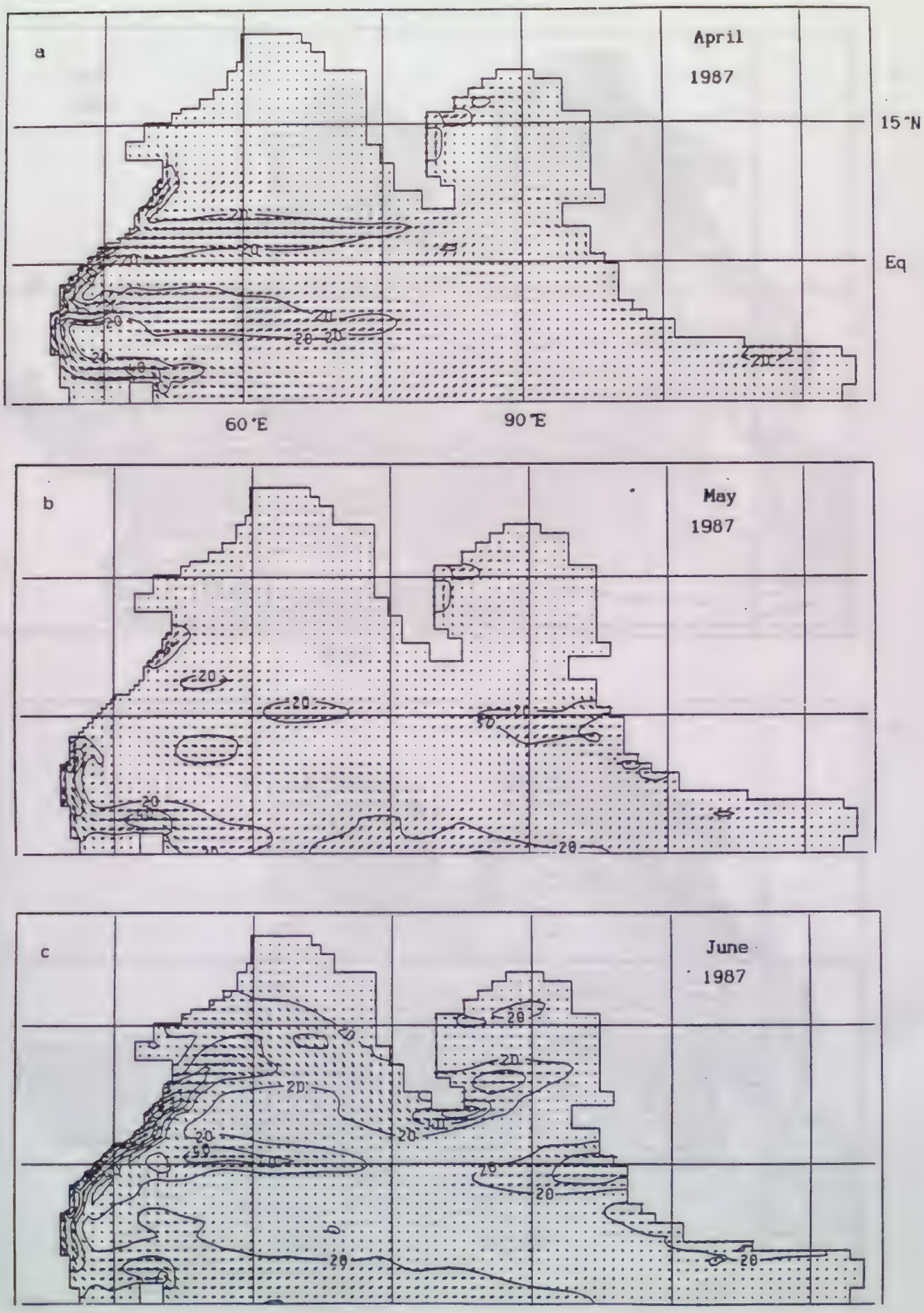

Fig.3.3 As Fig.3.2 but for 1988.

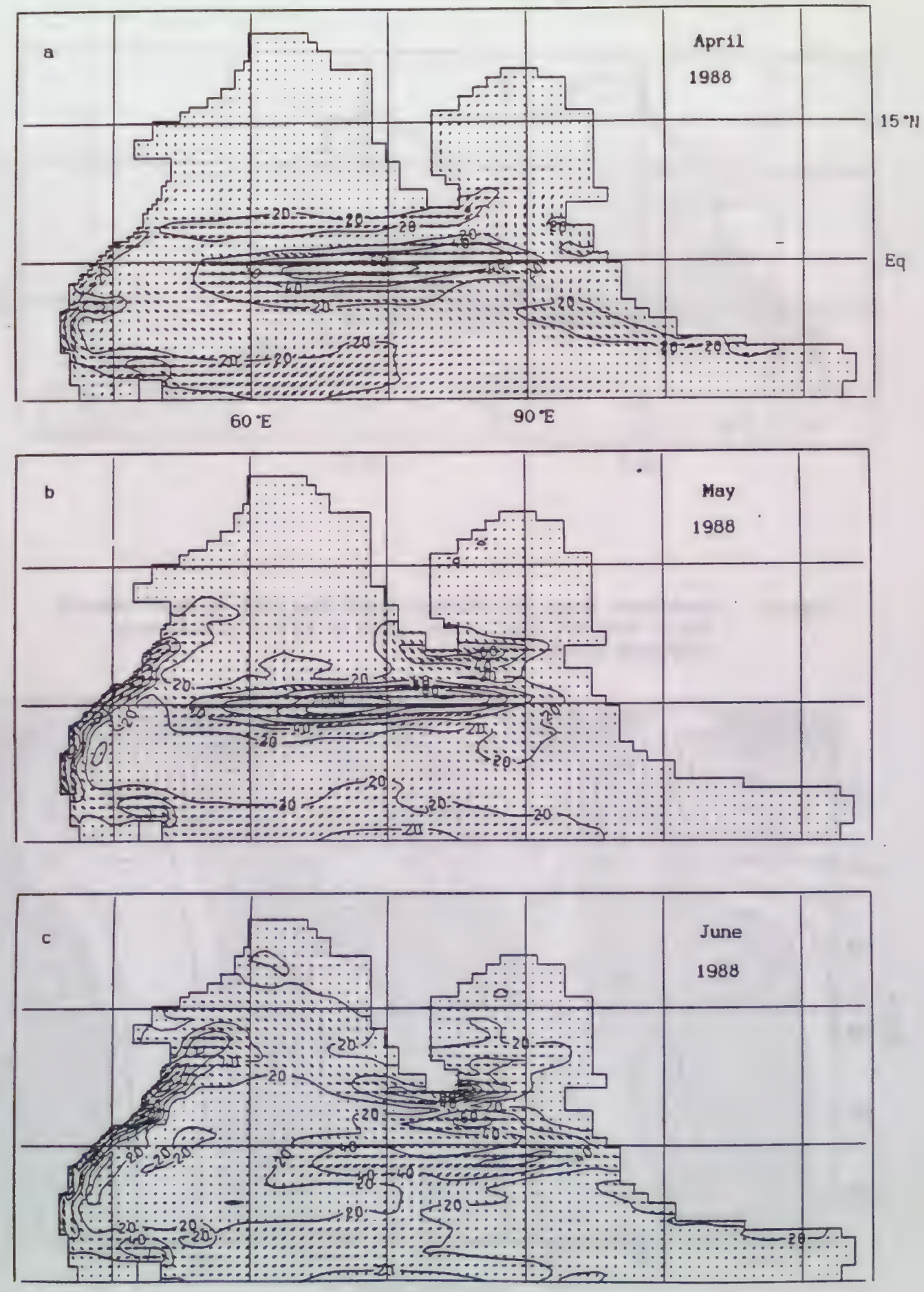

Fig.3.4 Experiment using MO stresses: difference chart of 5m currents (cm/s) for May 1988 minus May 1987.

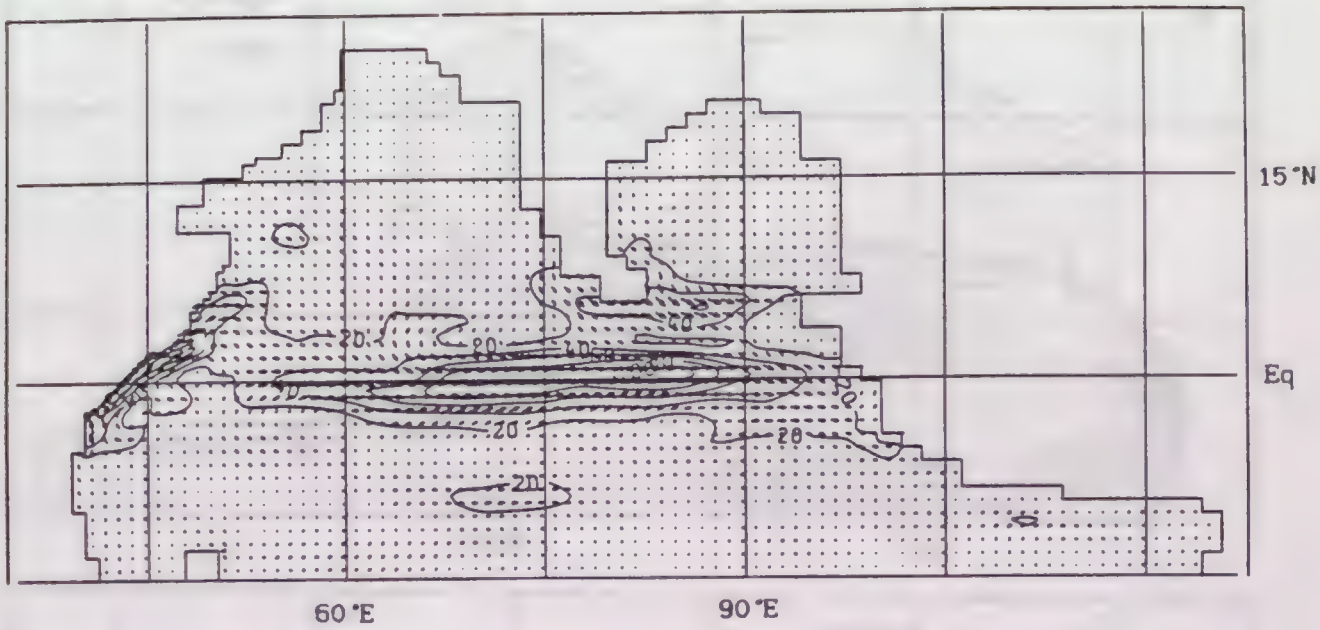

Fig.3.5 Experiment using MO stresses: depth-time plot of zonal velocity (cm/s) from Jan. 1987 to Dec. 1988 at 73°E on the Equator (westward values shaded).

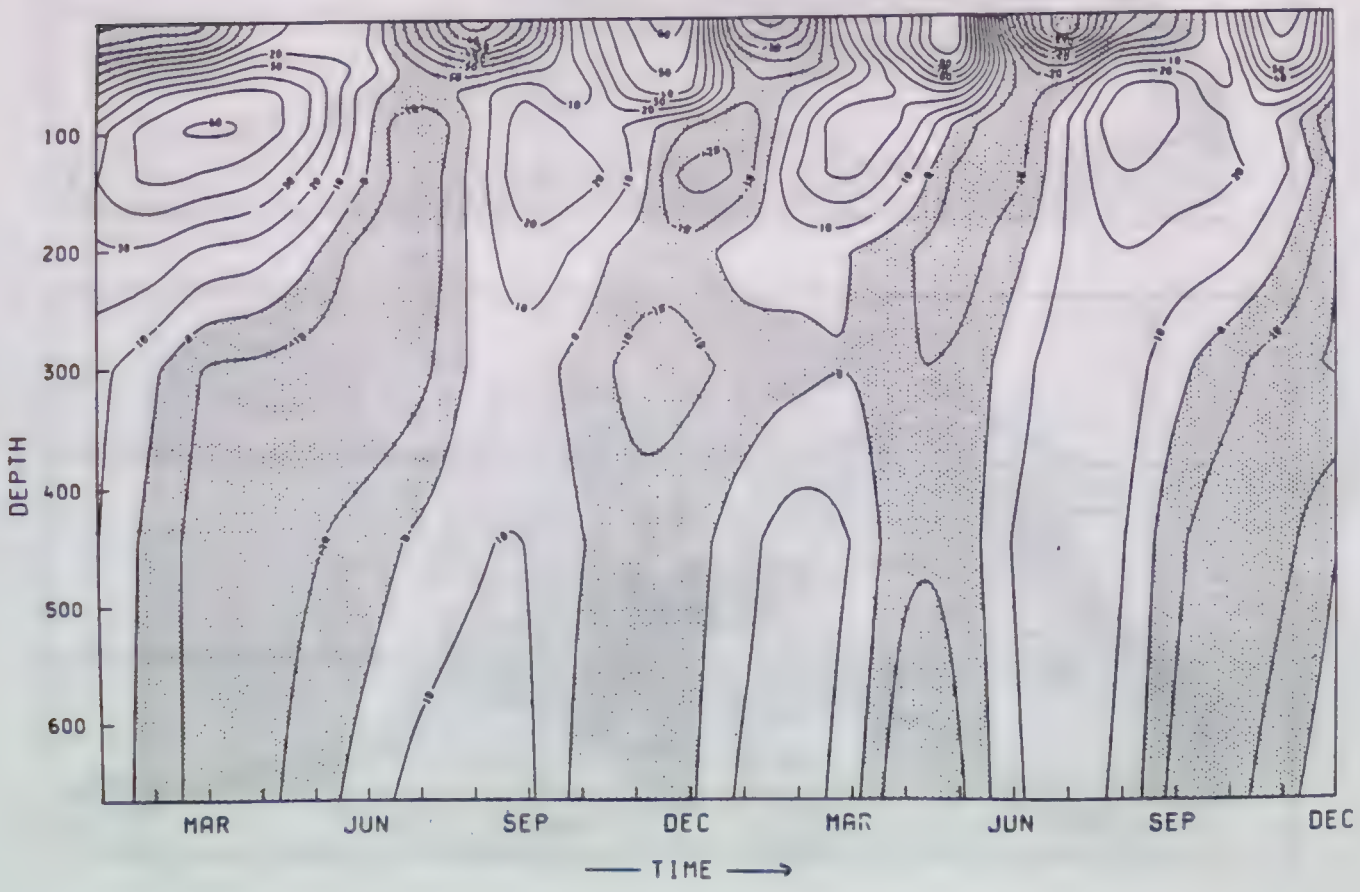

Fig.3.6 Experiment using MO stresses: 5m currents (cm/s) for (a) August 1987, (b) July 1988 and (c) July 1989.

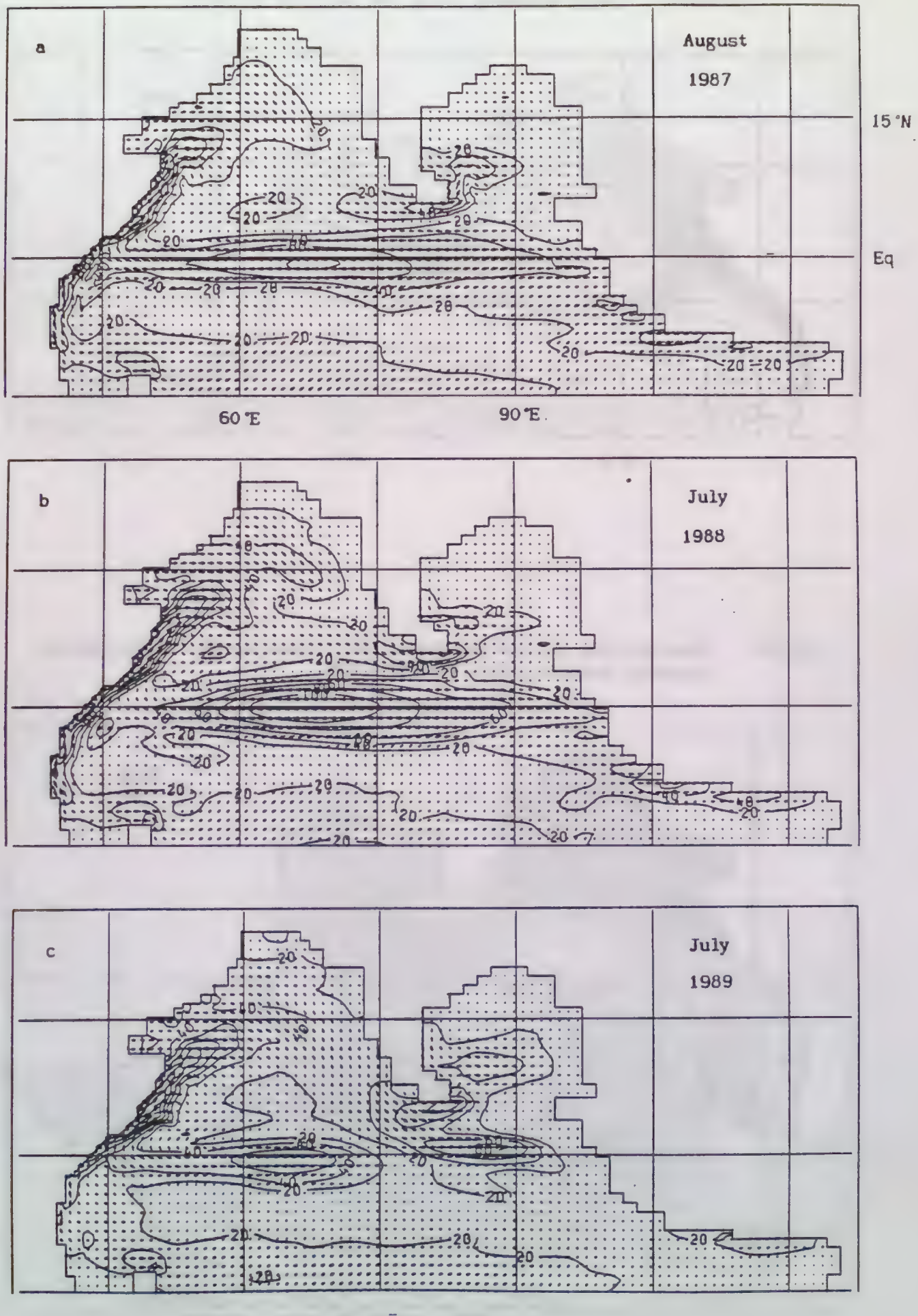

Fig.3.7 Model seasonal cycle: 5m currents for July.

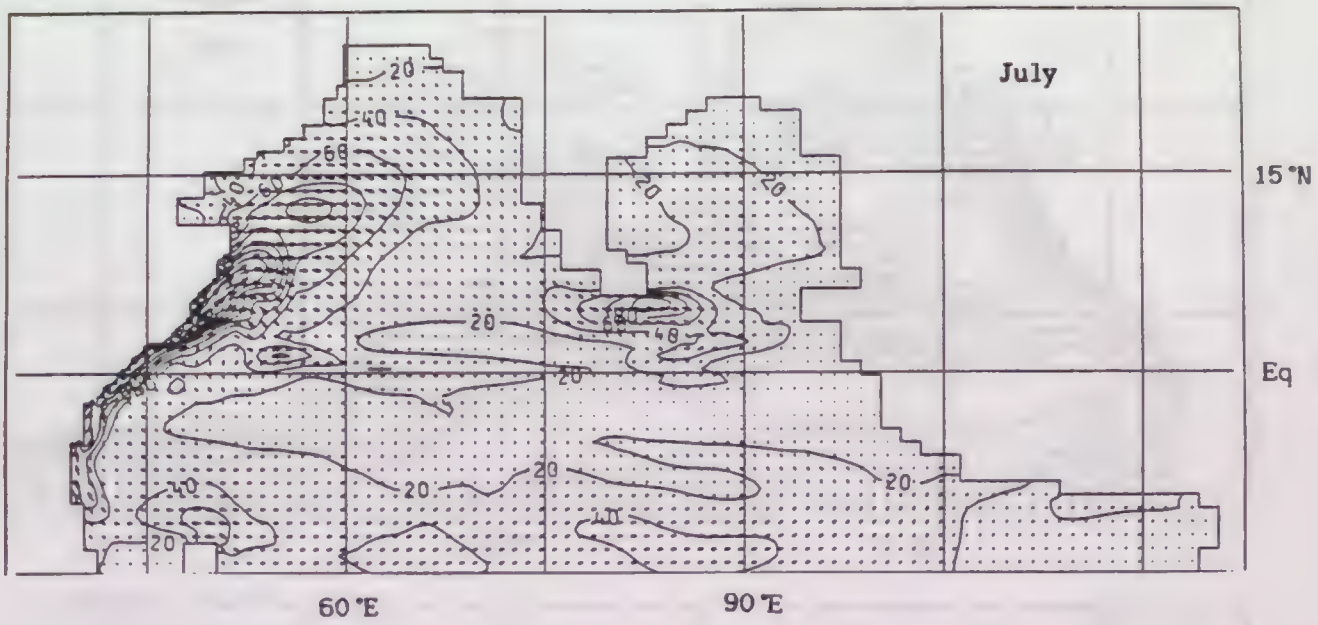

Fig.3.8 Mean-monthly wind-stress (dynes/cm²) from the Met. Office global forecast model analyses for July 1989.

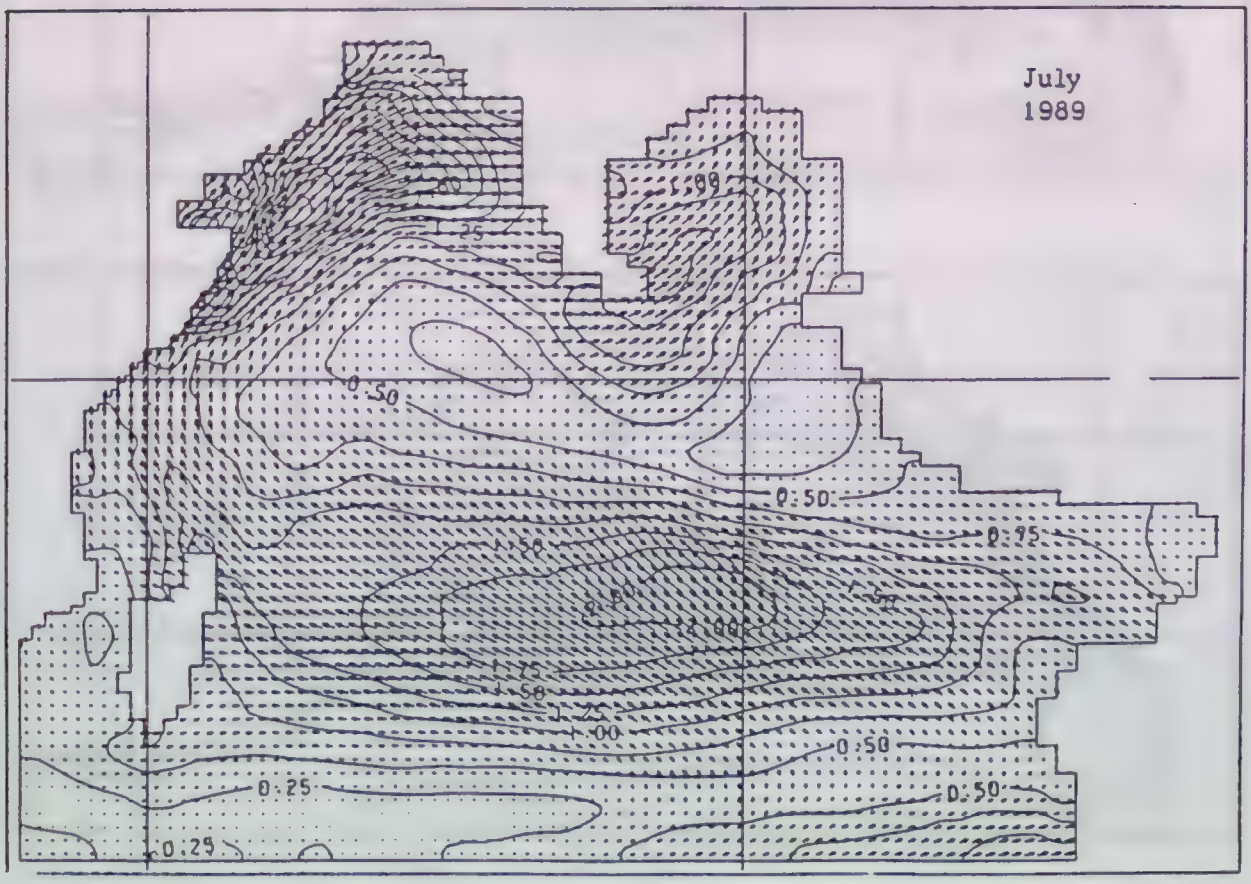

Fig.3.9 Surface zonal currents, u_s, and weekly-averaged zonal wind stress, τ_x, on the Equator at 73°E from January 1973 to September 1974. (From Knox, 1976)

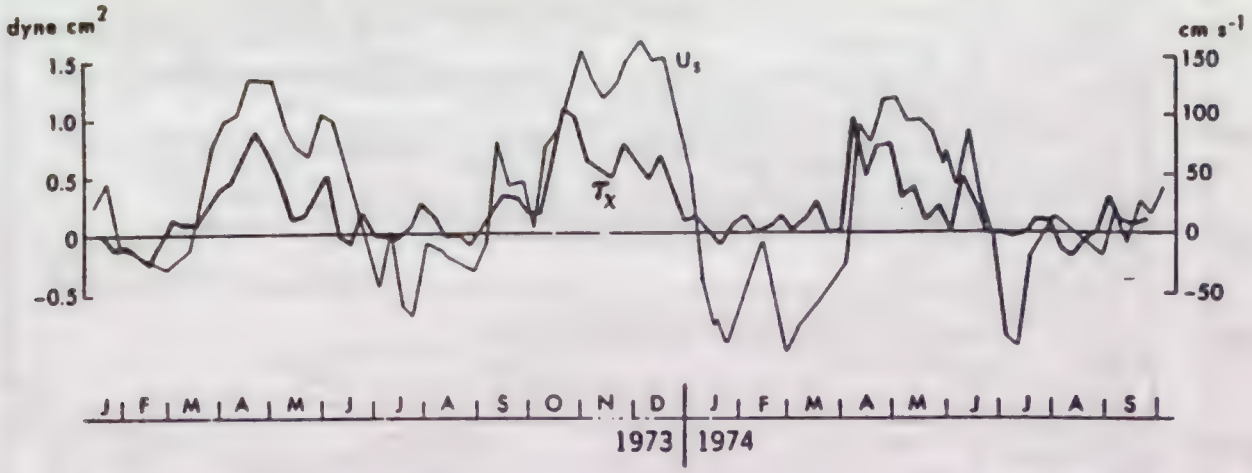

Fig.4.1 Time-longitude plot of zonal velocity (cm/s) at 5m depth on the Equator from Jan. 1987 to Dec. 1988 for (a) EXPMO, (b) EXPEC and (c) difference field EXPMO minus EXPEC. (Westward values shaded)

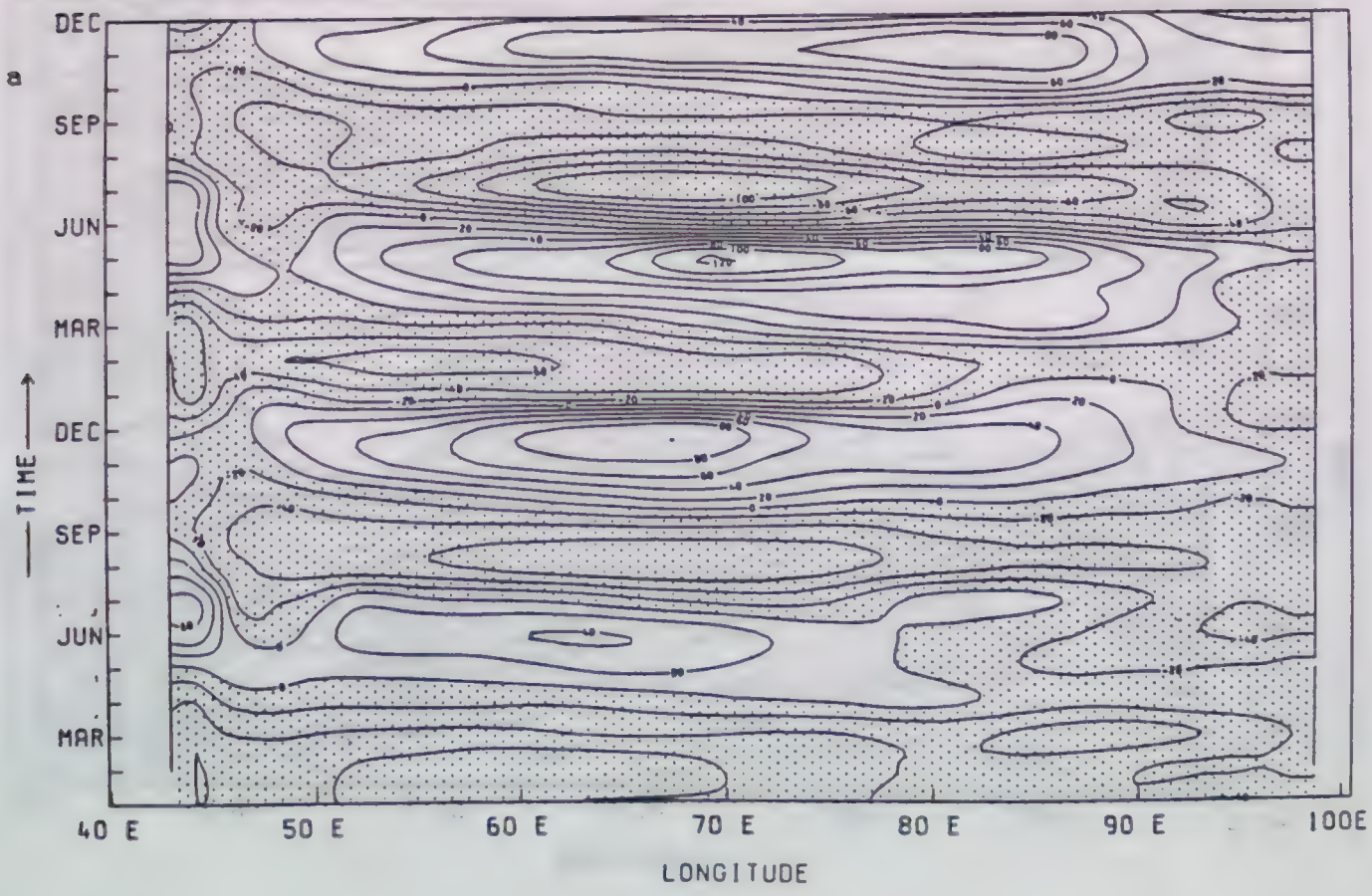

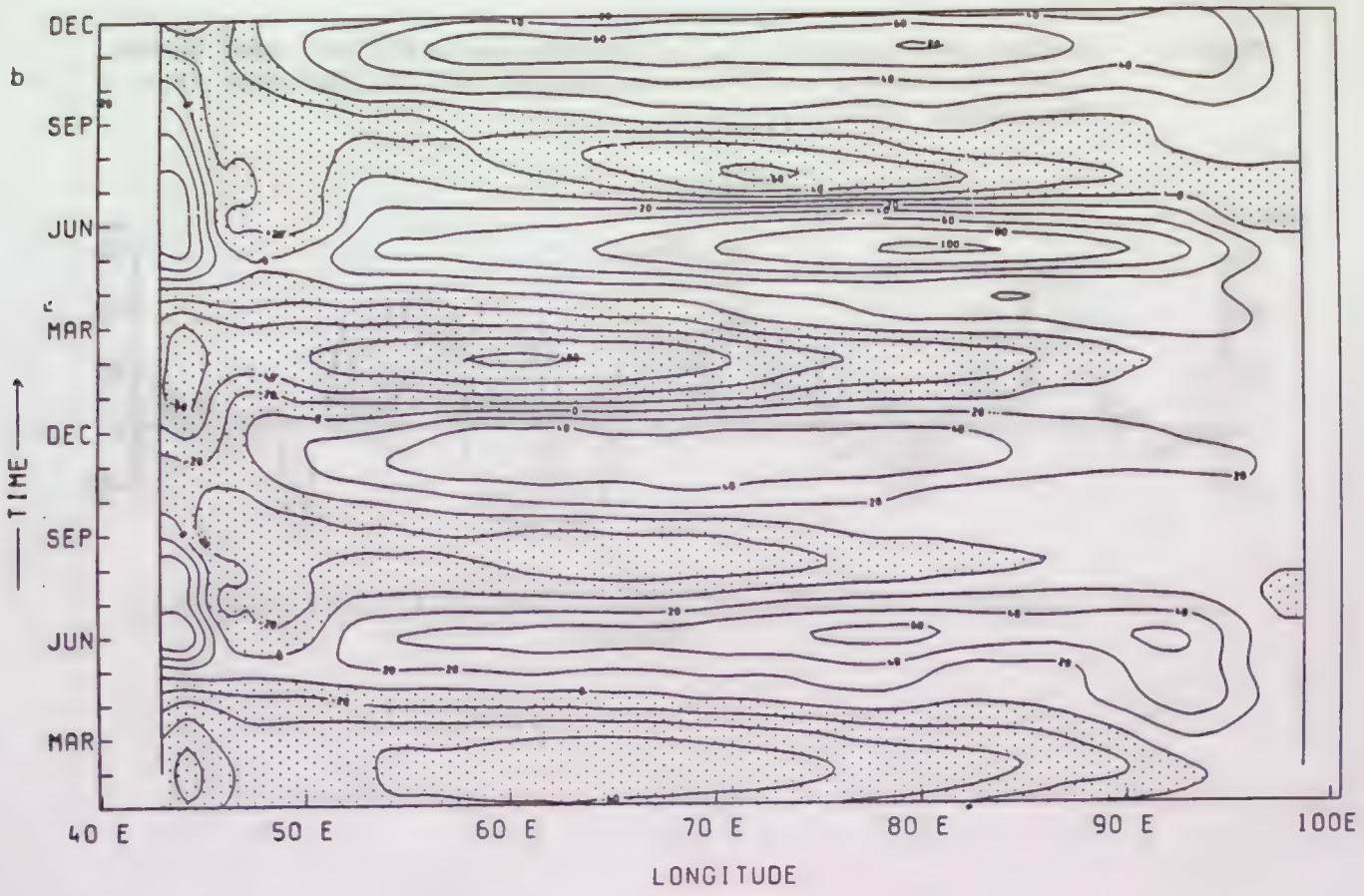
b
DEC
SEP
JUN
MAR
DEC
SEP
JUN
MAR
TIME
40 E
50 E
60 E
70 E
80 E
90 E
100E
LONGITUDE

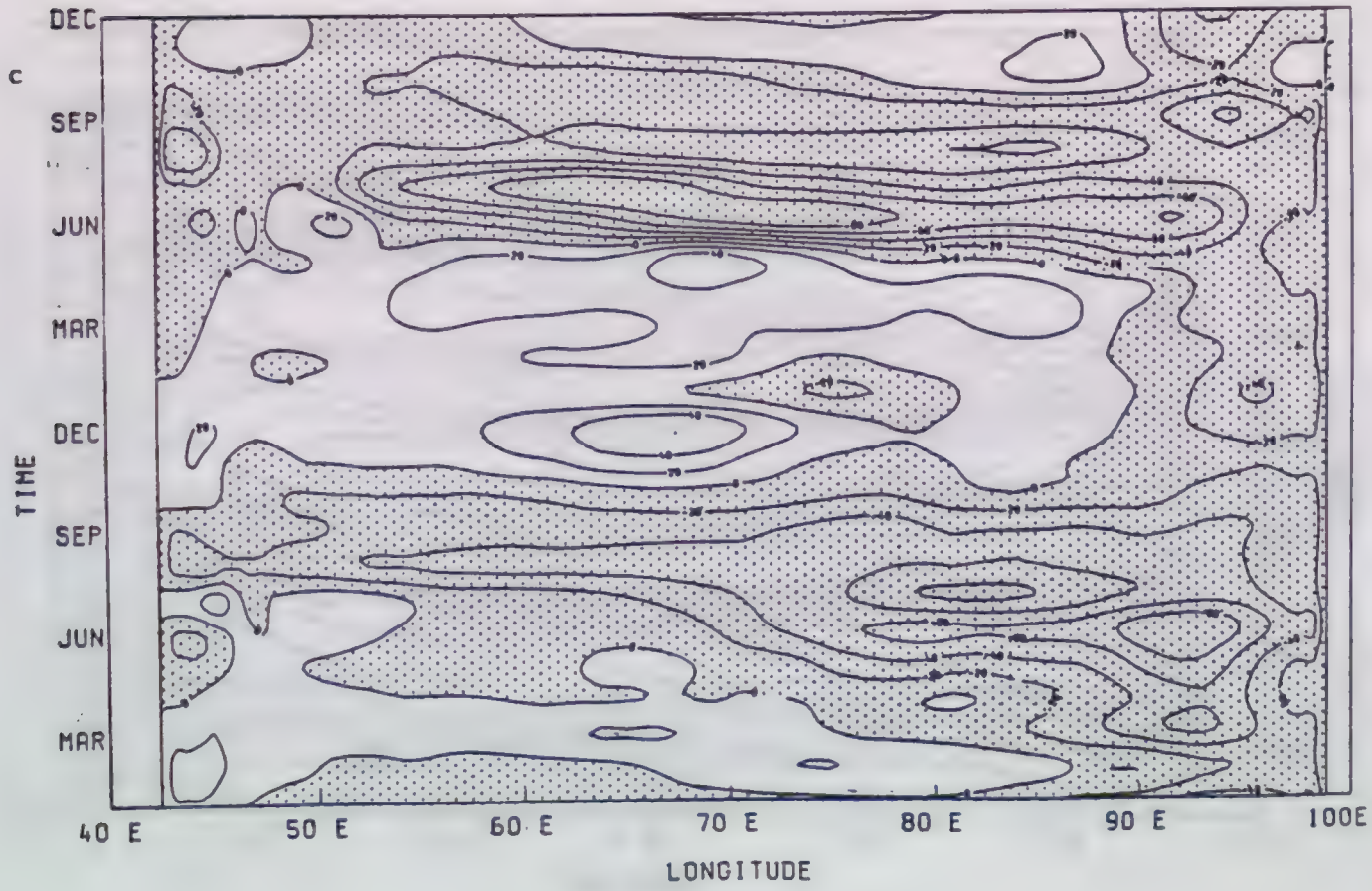
c
DEC
SEP
JUN
MAR
DEC
SEP
JUN
MAR
TIME
40 E
50 E
60 E
70 E
80 E
90 E
100E
LONGITUDE

Fig.4.2 EXPEC: 5m currents (cm/s) for July 1988.

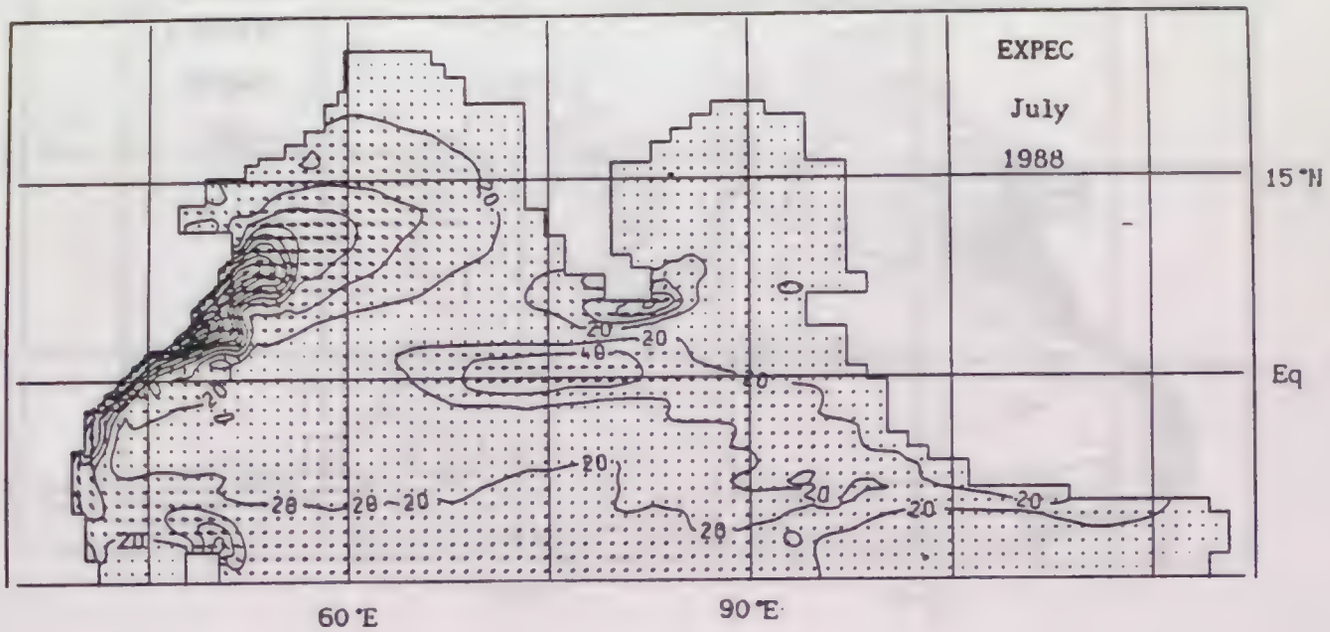

Fig.4.3 Difference chart of 5m currents (cm/s), EXPEC minus EXPMO, for July 1988.

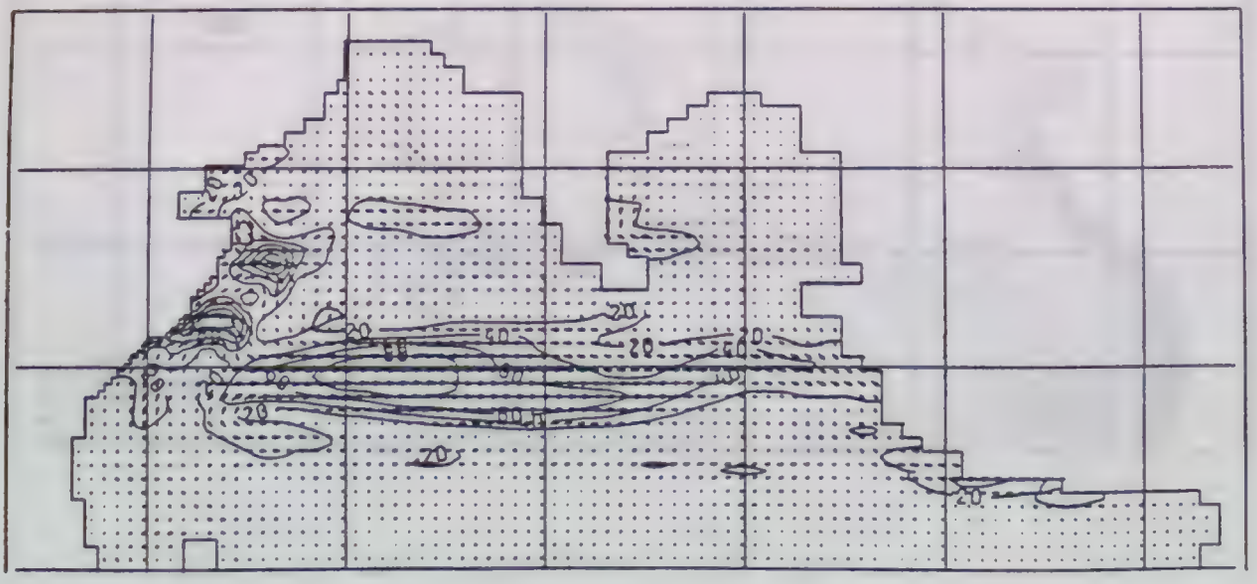

Fig.4.4 As Fig.4.2 but for August 1987.

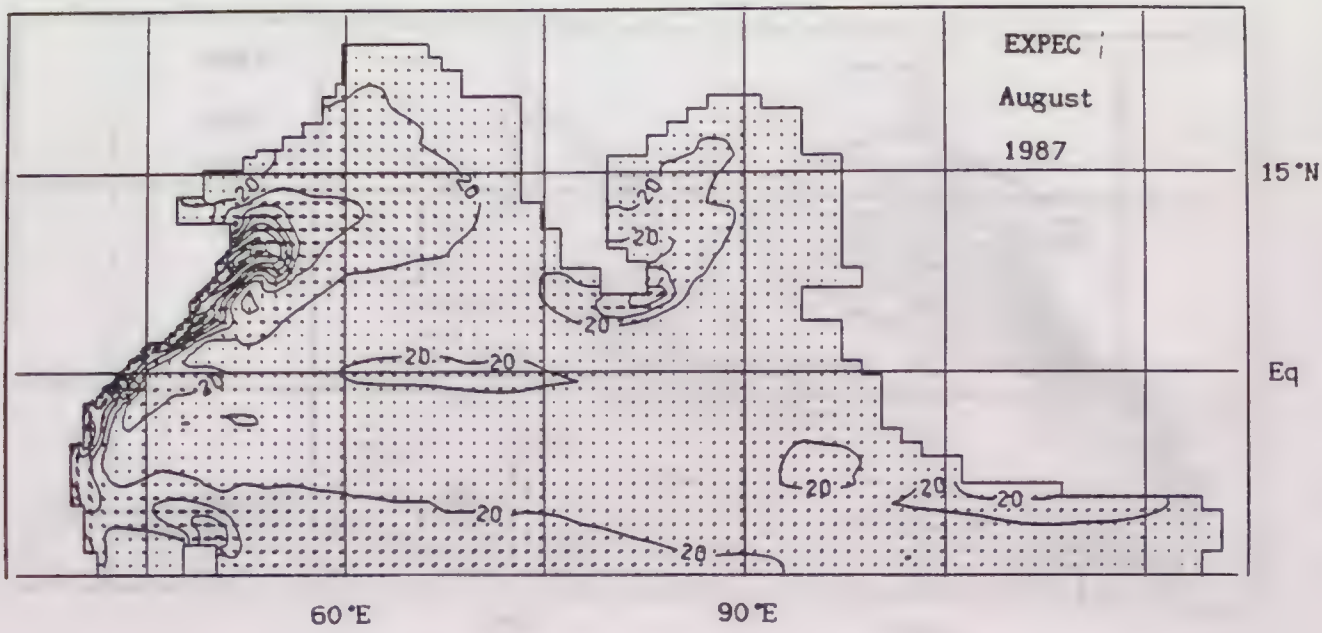

Fig.4.5 As Fig.4.2 but for May 1987.

Fig.4.6 EXPEC: depth-time plot of zonal velocity (cm/s) from Jan. 1987 to Dec. 1988 at 73°E on the Equator (westward values shaded).

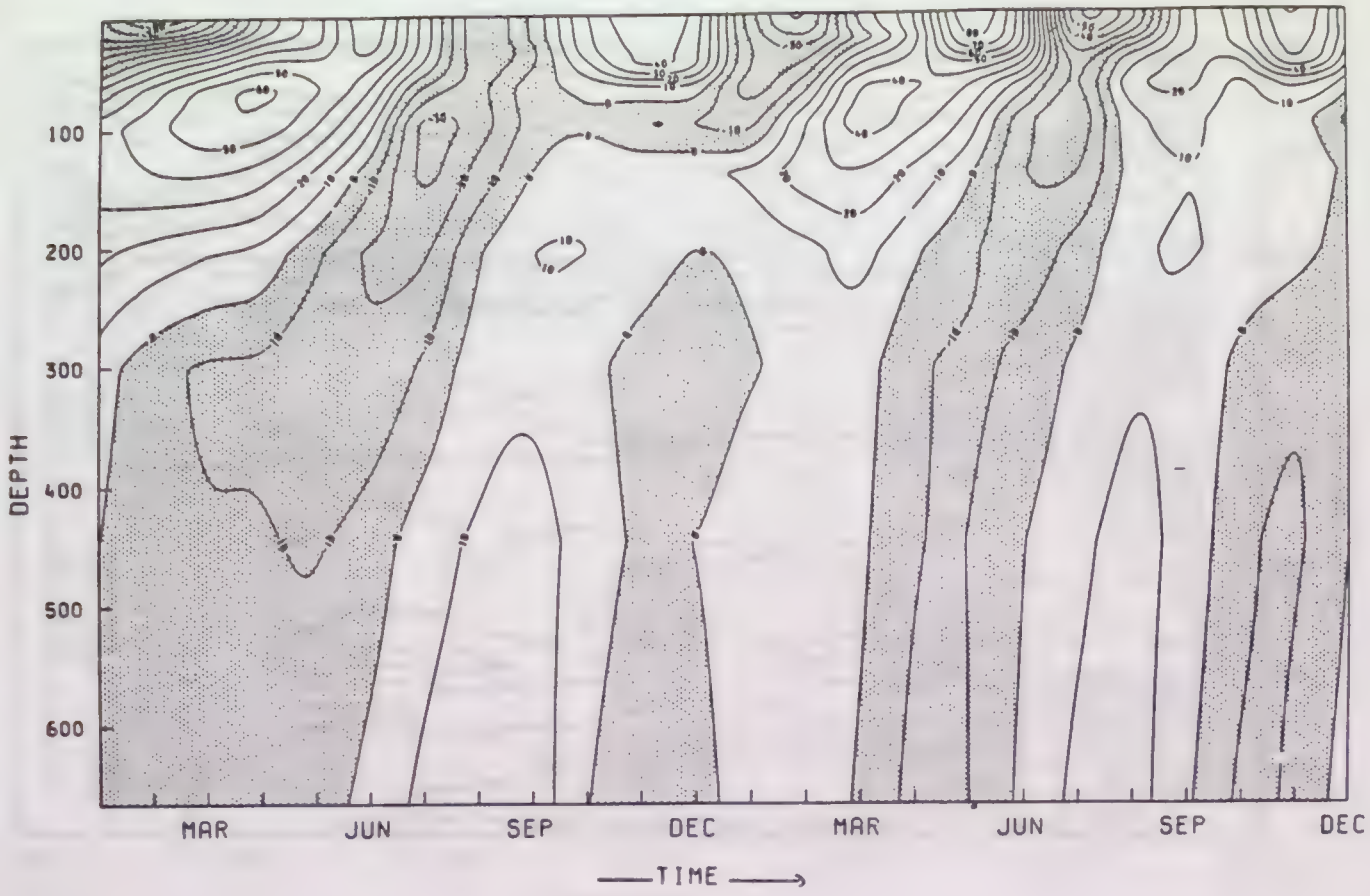

Fig.4.7 Time-longitude plot of zonal wind stress (dynes/cm^2) on the Equator from Jan. 1987 to Dec. 1988 for (a) EXPMO, (b) EXPEC and (c) difference field EXPMO minus EXPEC. (Westward values shaded)

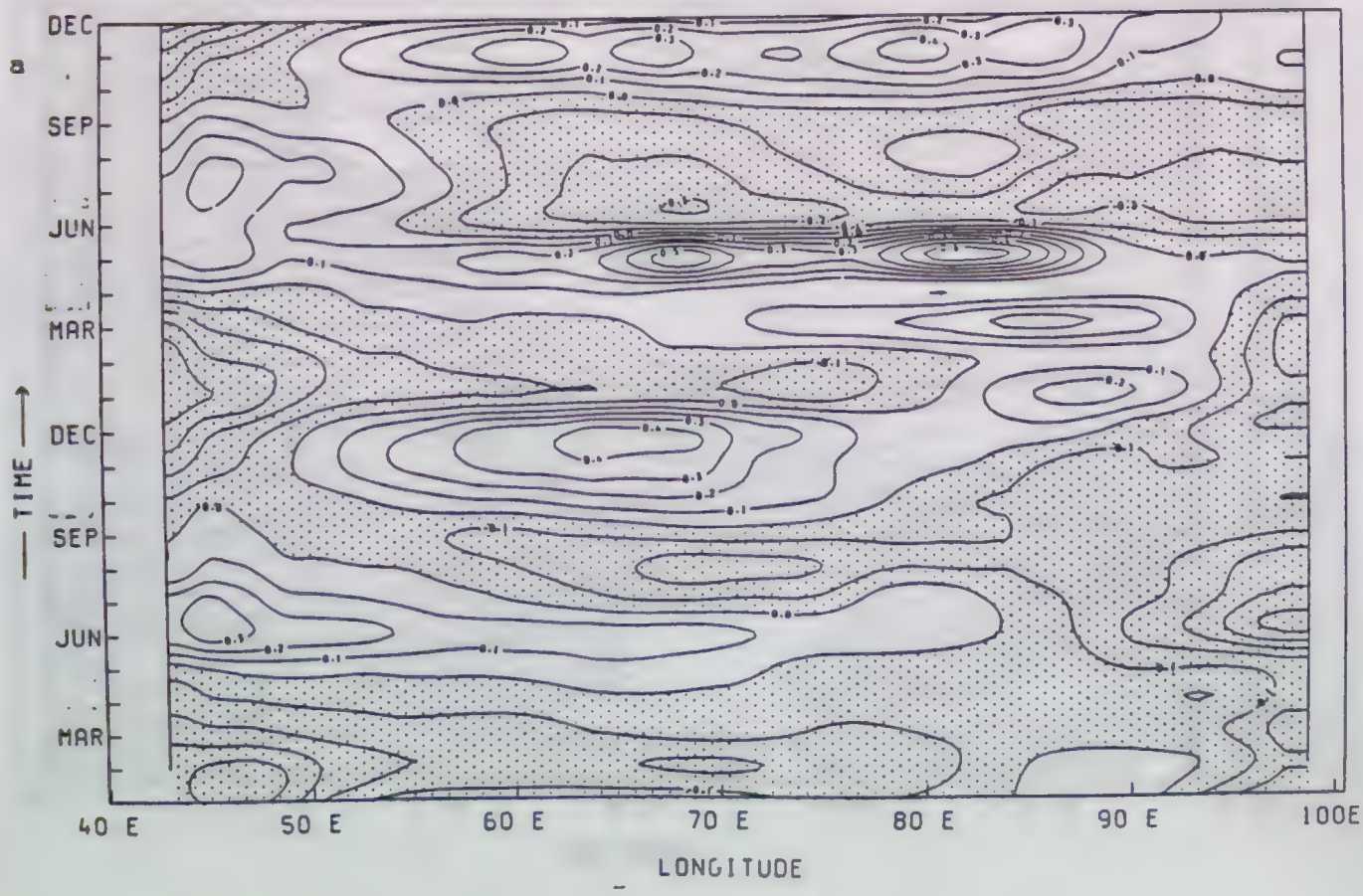

b

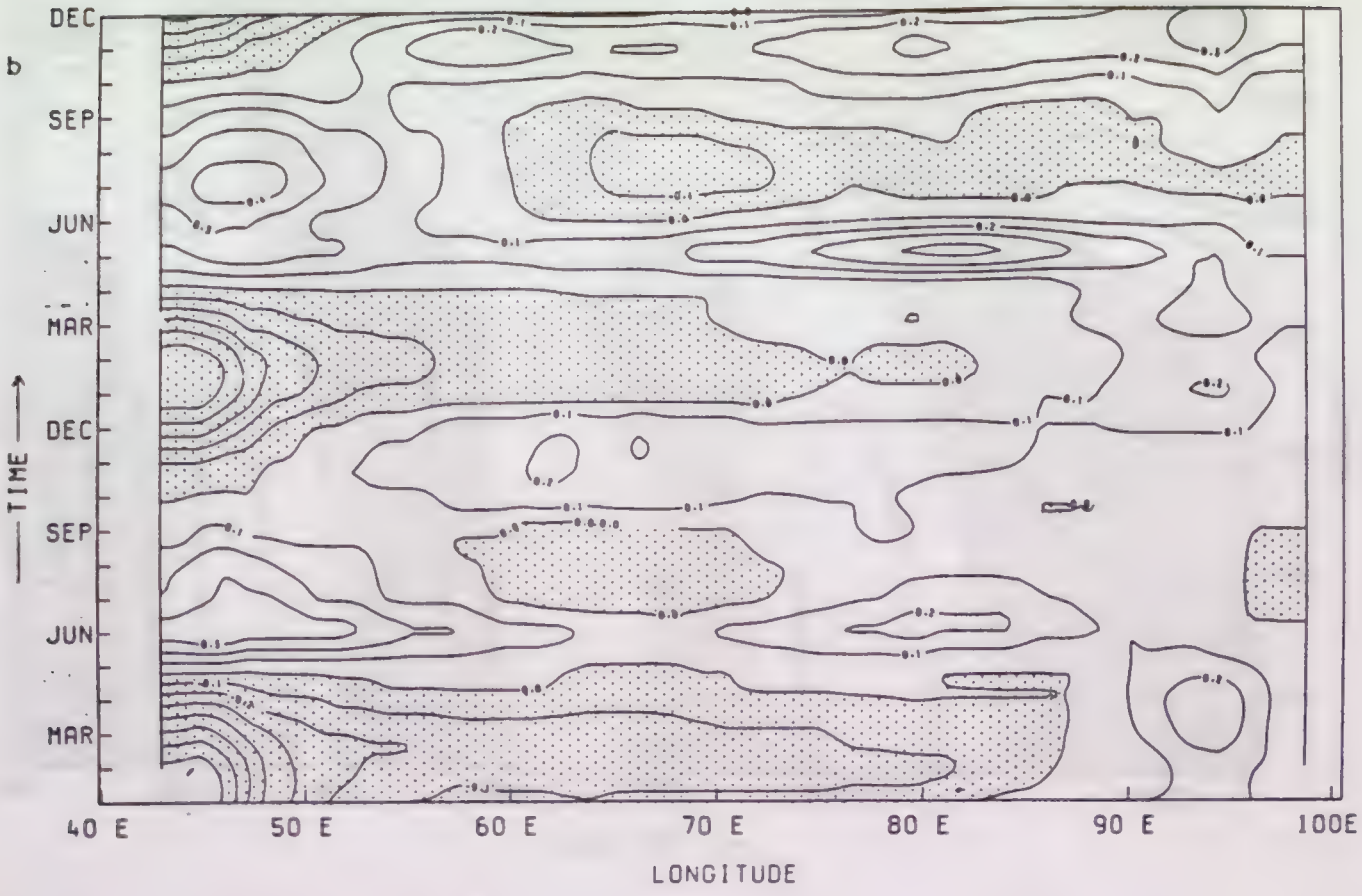
DEC
SEP
JUN
MAR
DEC
SEP
JUN
MAR
TIME
40 E
50 E
60 E
70 E
80 E
90 E
100E
LONGITUDE

c

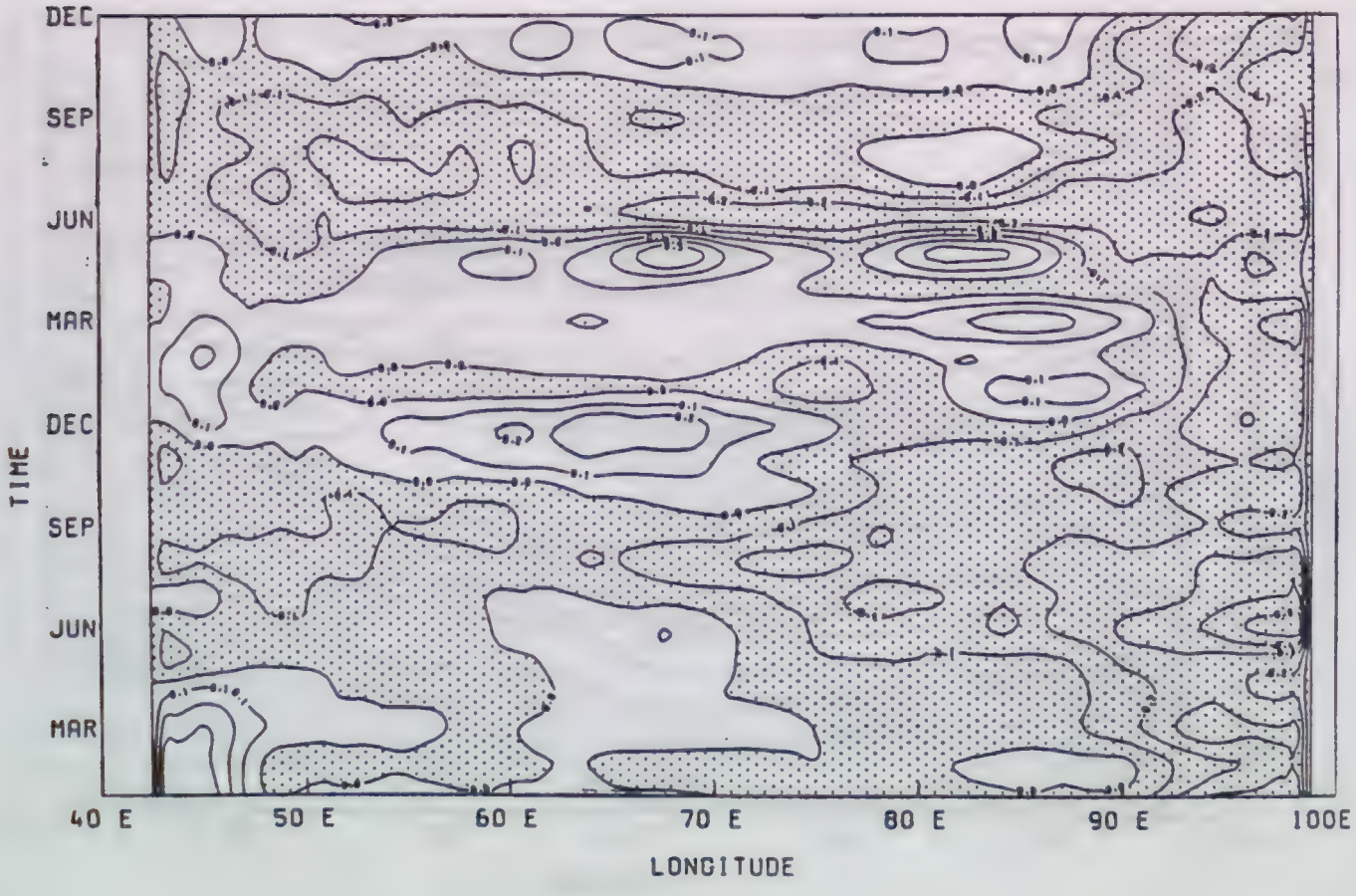
DEC
SEP
JUN
MAR
DEC
SEP
JUN
MAR
TIME
40 E
50 E
60 E
70 E
80 E
90 E
100E
LONGITUDE

Fig.5.1 Dynamic Height (dyn cm) for November 1987 from (a) EXPMO, (b) EXPEC and (c) Geosat altimeter analysis. (Contour interval 4 dyn cm, negative values shaded)

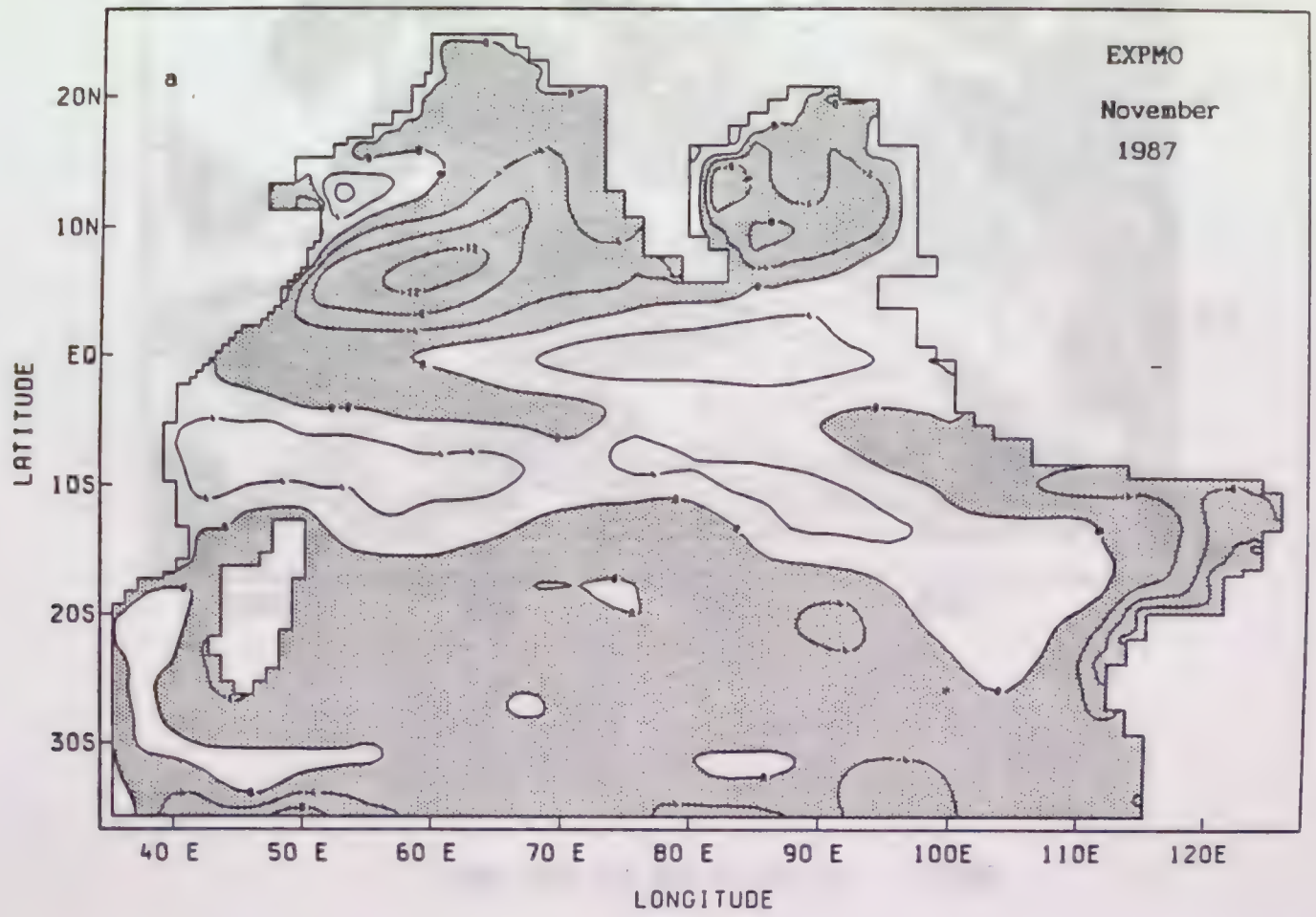

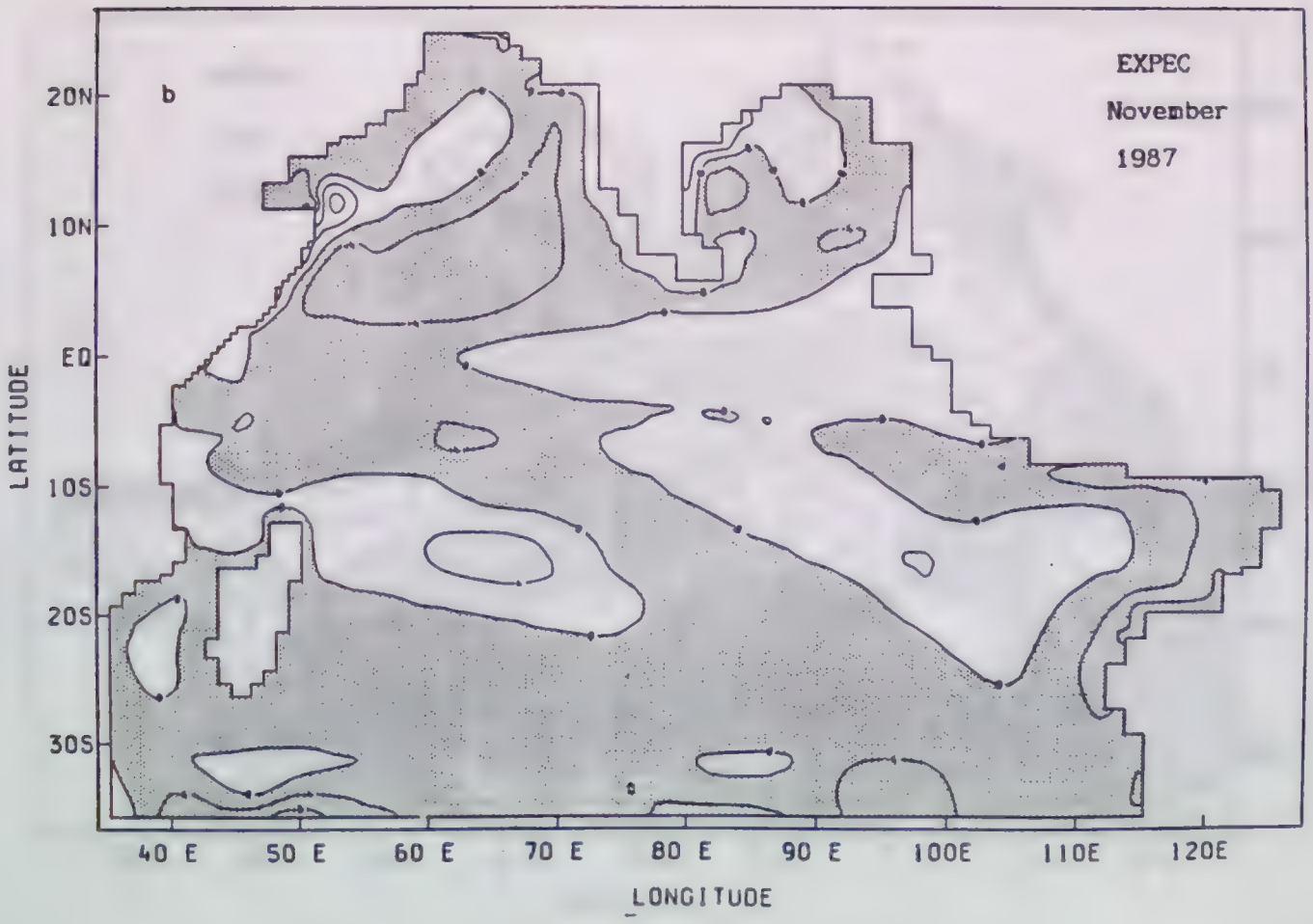

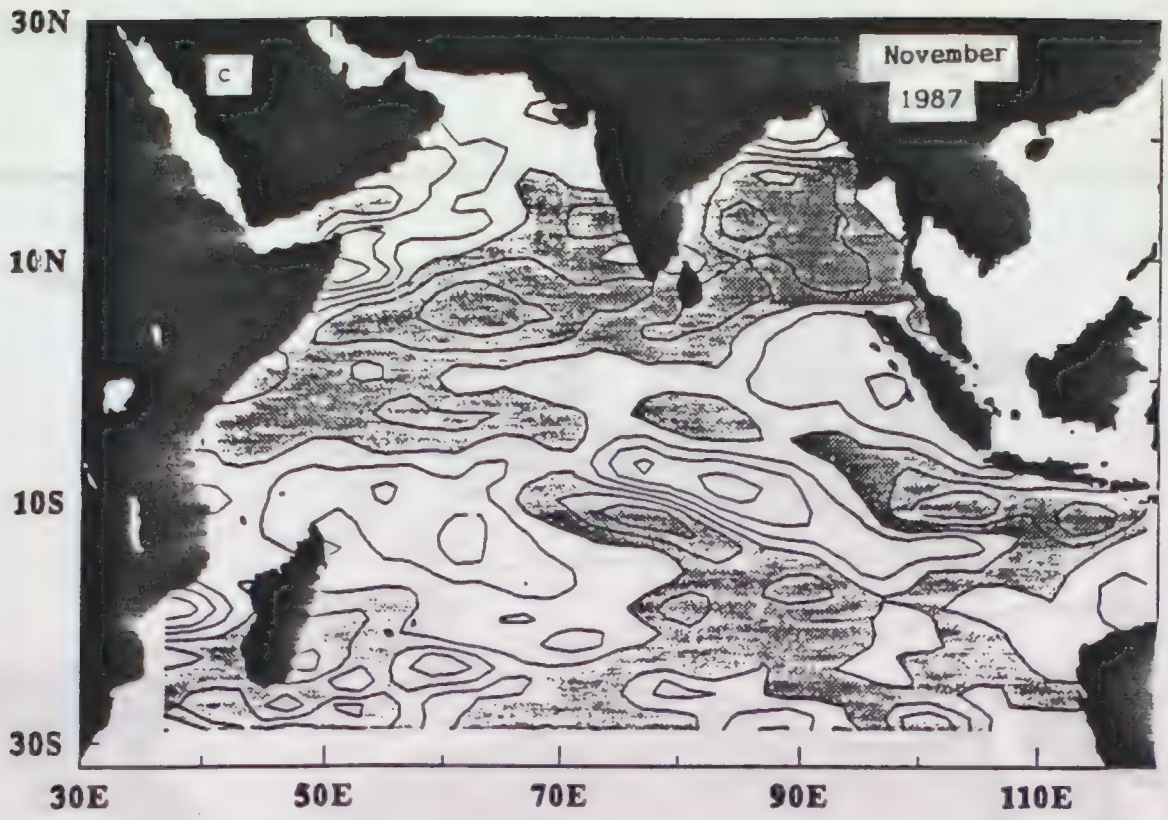

Fig.5.2 As Fig.5.1 but for July 1988.

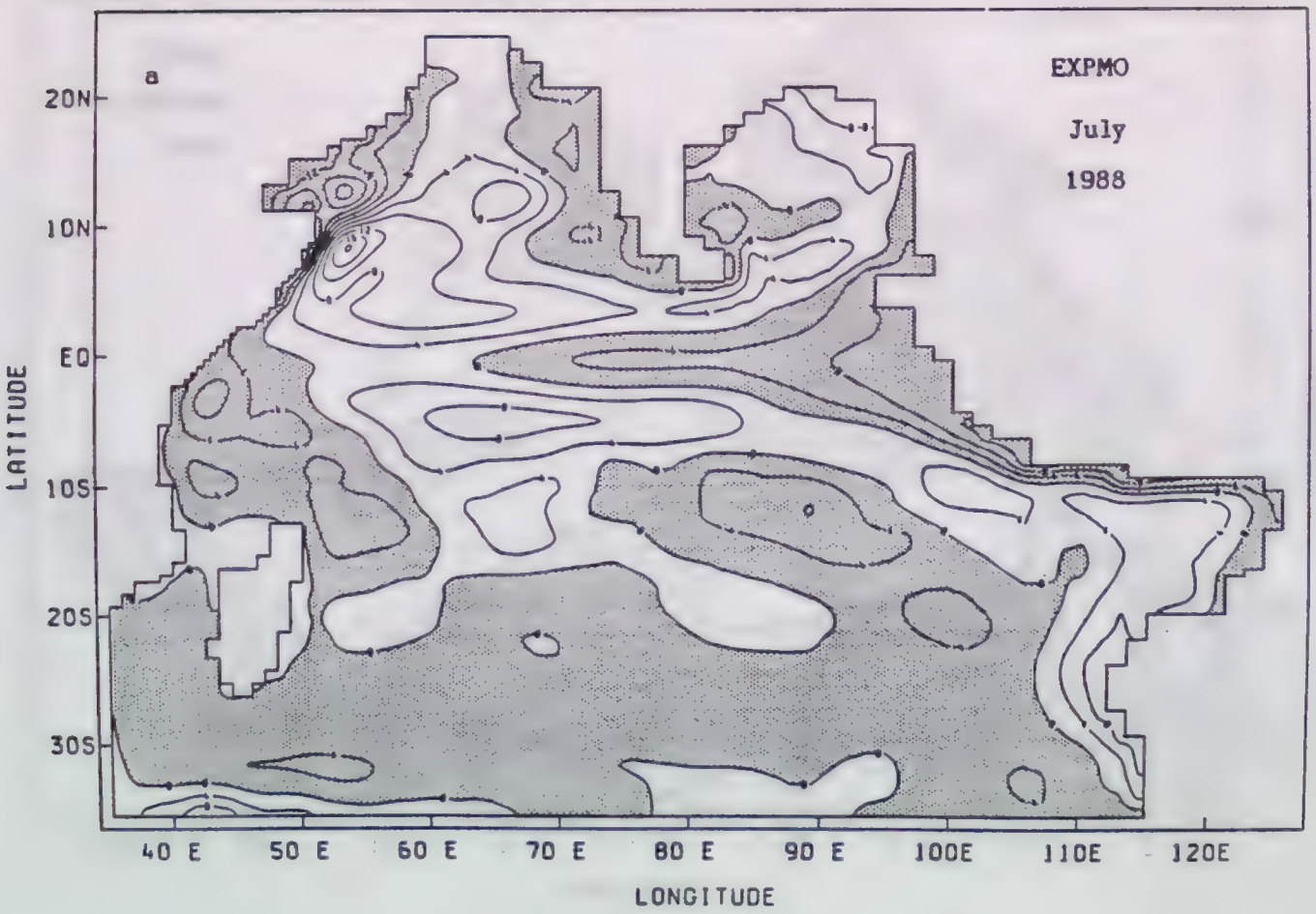

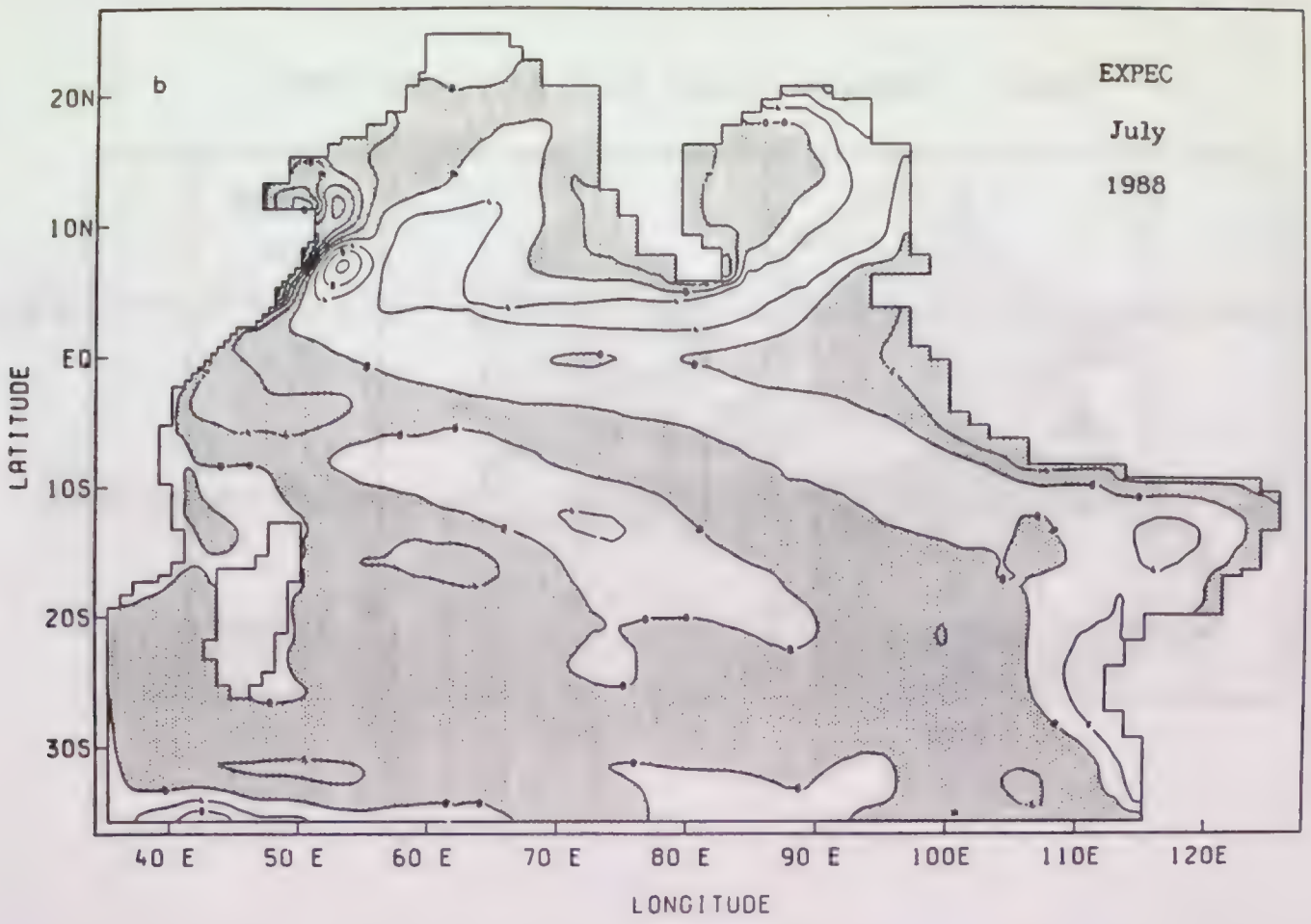
b
EXPEC
July
1988
20N
10N
EQ
10S
20S
30S
LATITUDE
40 E
50 E
60 E
70 E
80 E
90 E
100E
110E
120E
LONGITUDE

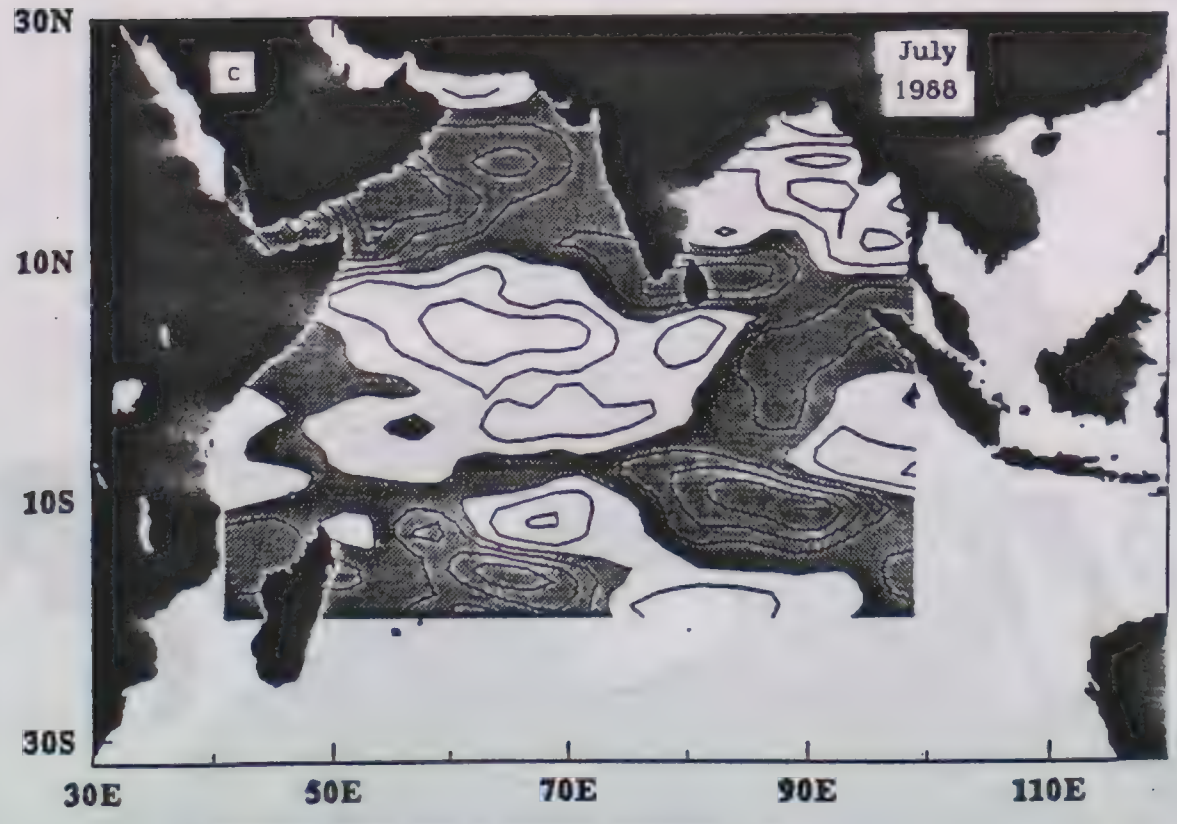
c
July
1988
30N
10N
10S
30S
30E
50E
70E
90E
110E

Fig.5.3 EXPMO: 5m currents (cm/s) for November 1987.

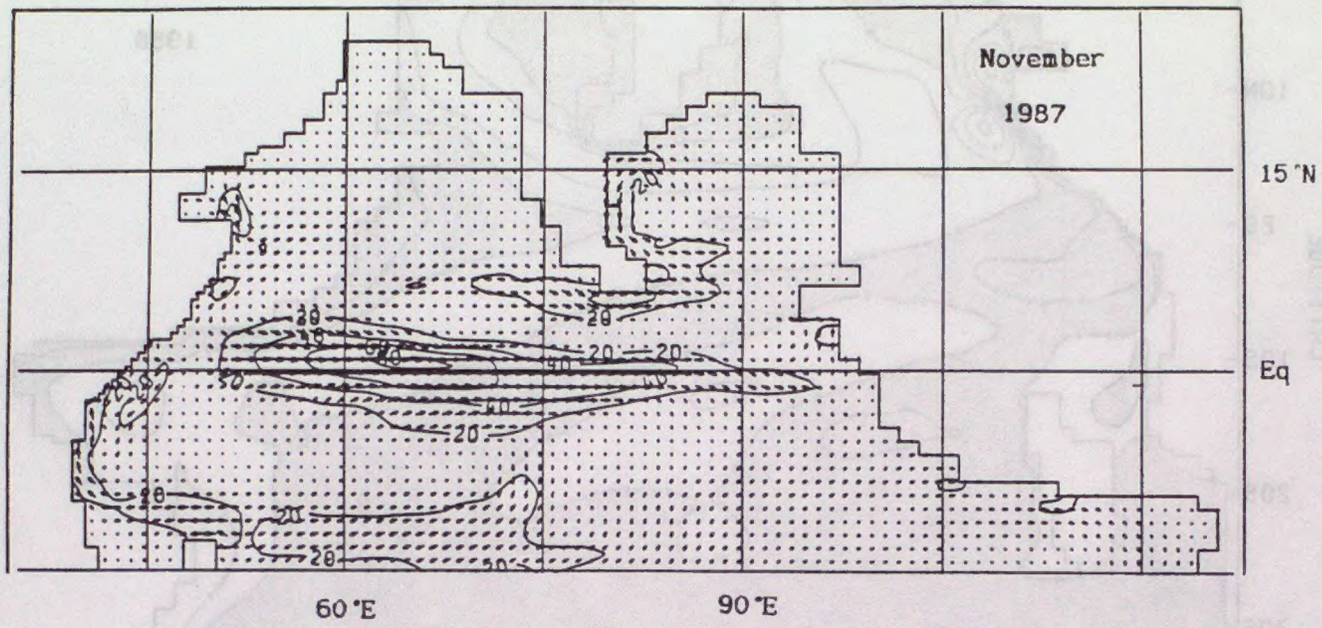

Fig.5.4 As Fig.5.1 but for November 1988.

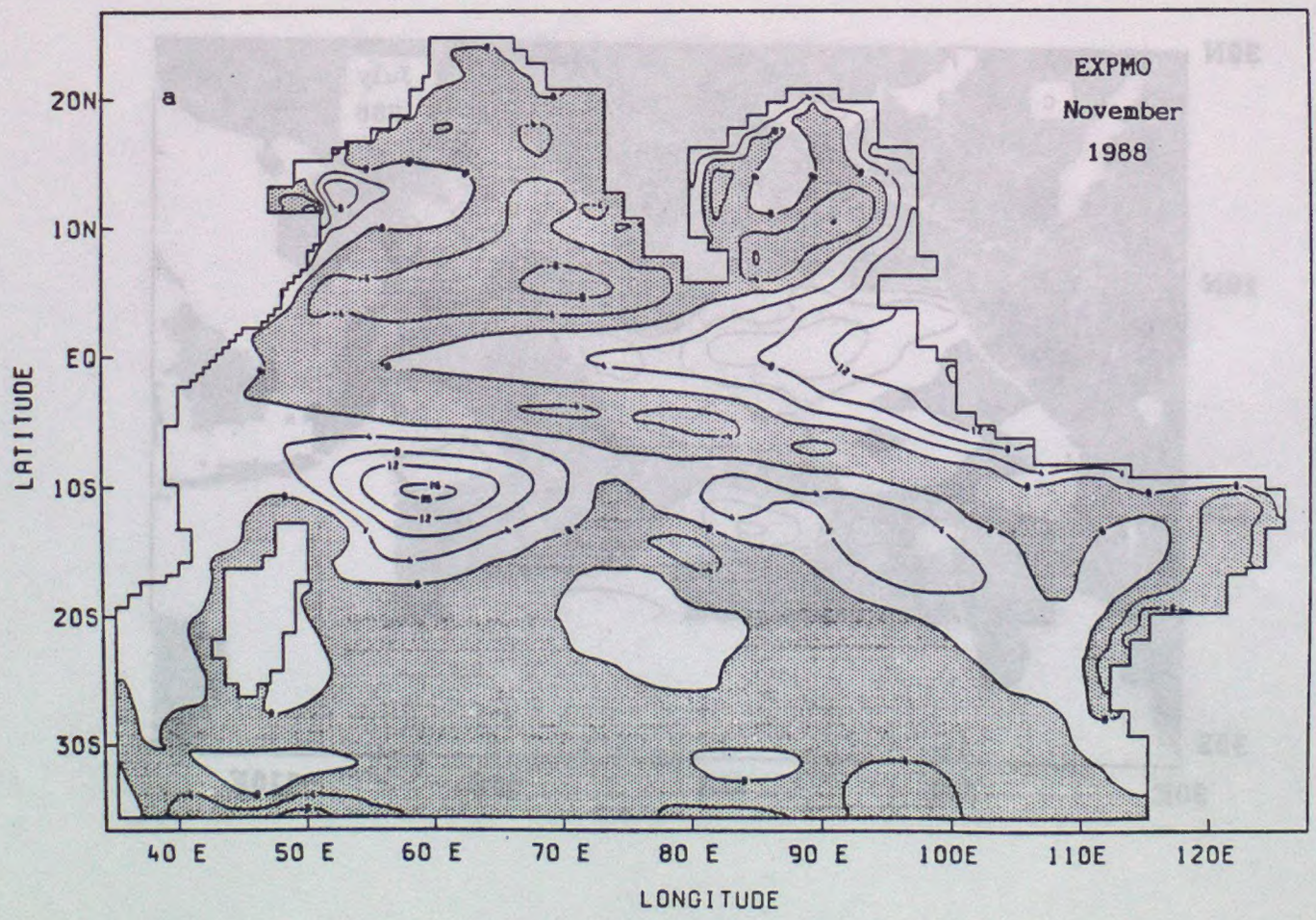

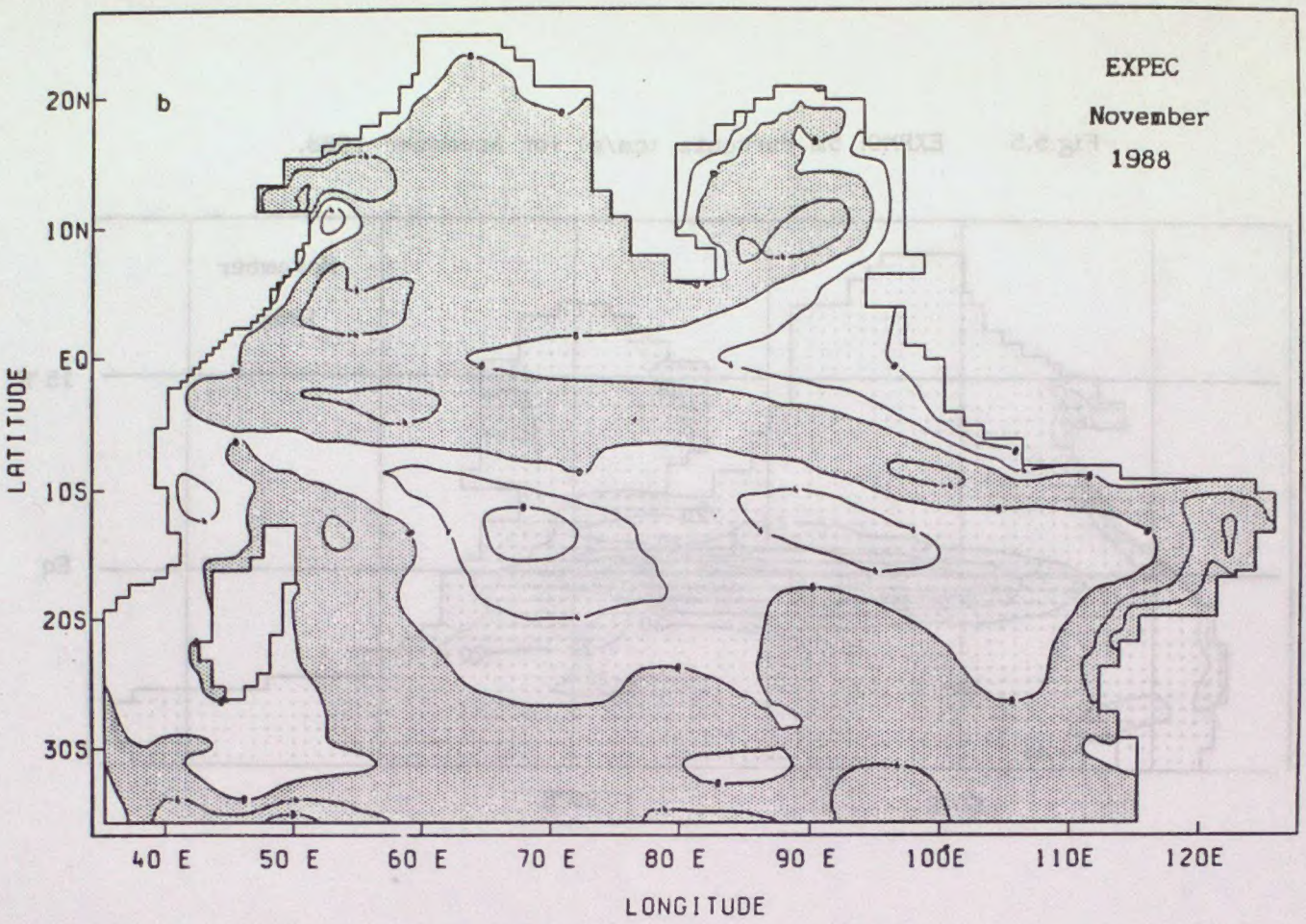
b
EXPEC
November
1988
20N
10N
EQ
10S
20S
30S
LATITUDE
40 E
50 E
60 E
70 E
80 E
90 E
100E
110E
120E
LONGITUDE

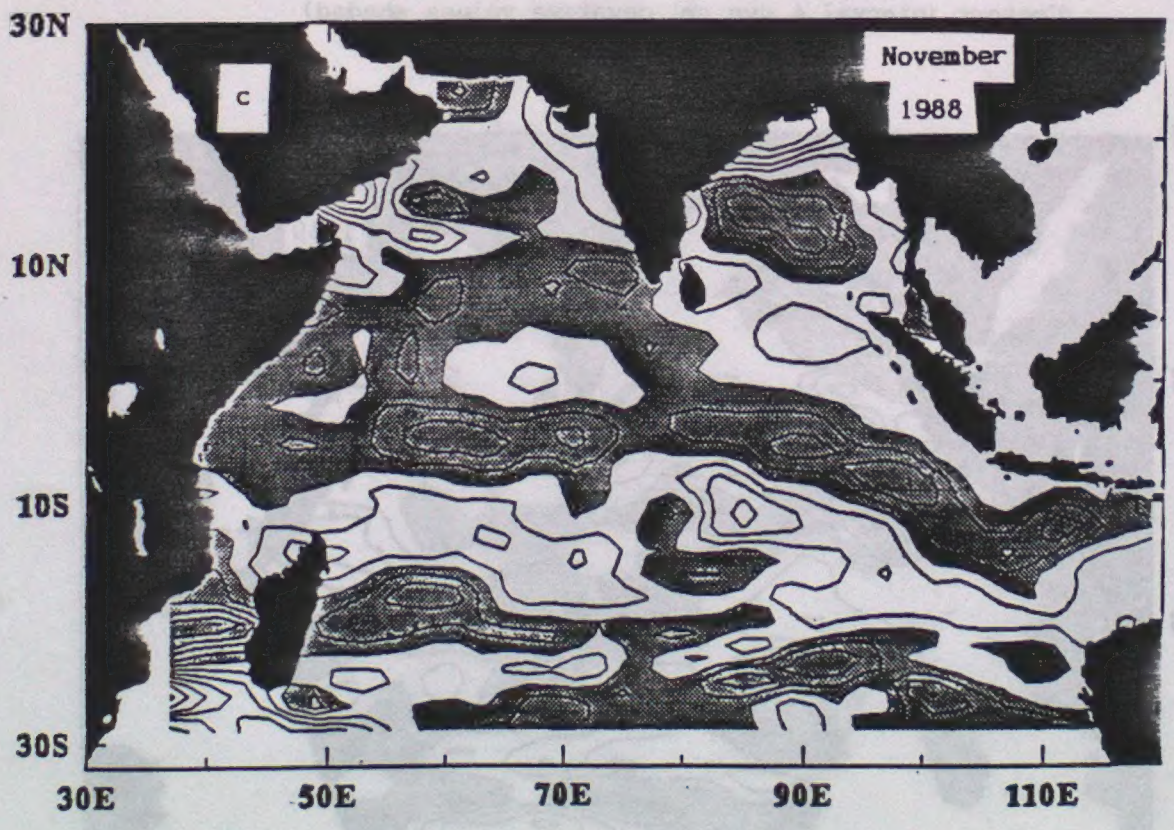
c
November
1988
30N
10N
10S
30S
30E
50E
70E
90E
110E

Fig.5.5 EXPMO: 5m currents (cm/s) for November 1988.

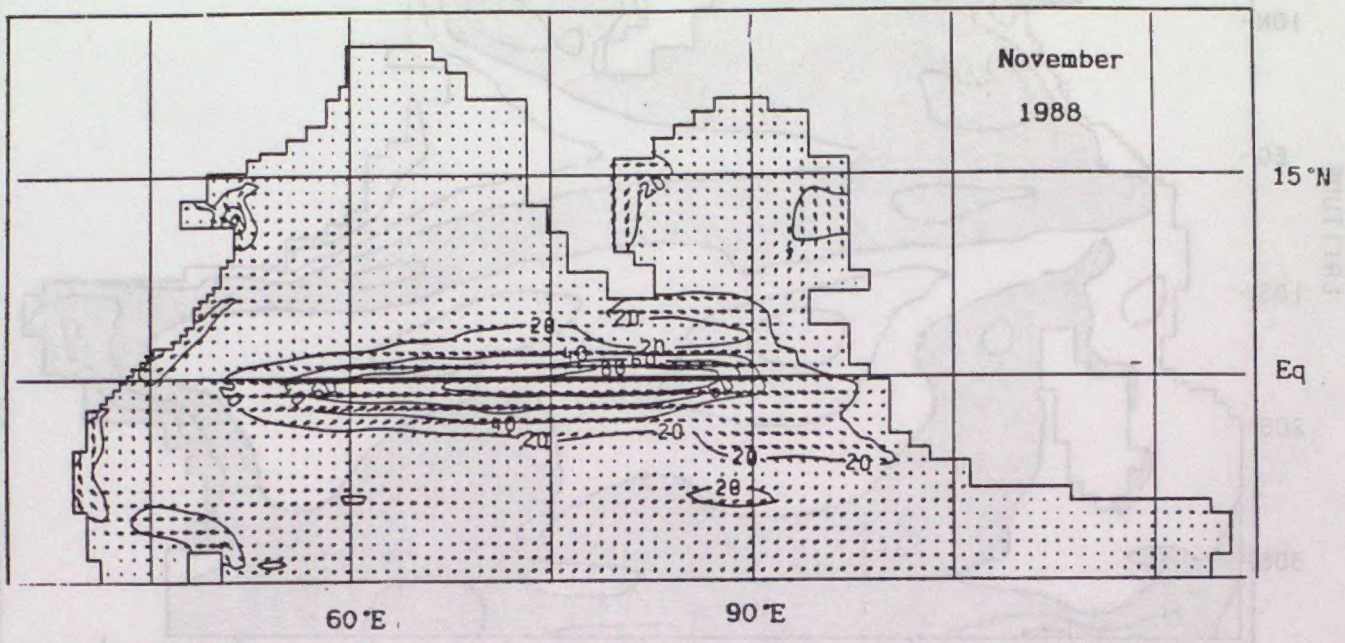

Fig.5.6 Dynamic Height (dyn cm) for July 1989 from Geosat altimeter analysis. (Contour interval 4 dyn cm, negative values shaded)

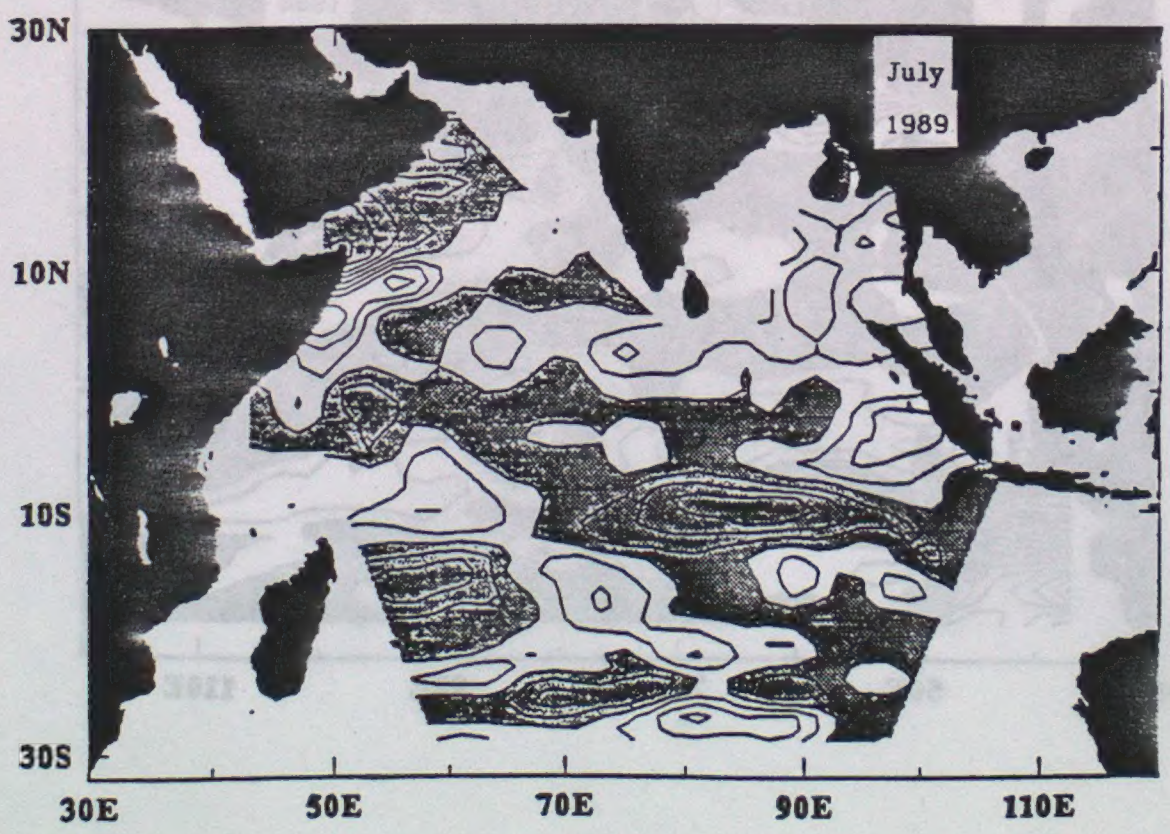

CLIMATE RESEARCH TECHNICAL NOTES

CRTN 1	Oct 1990	Estimates of the sensitivity of climate to vegetation changes using the Penman-Monteith equation. P R Rowntree
CRTN 2	Oct 1990	An ocean general circulation model of the Indian Ocean for hindcasting studies. D J Carrington
CRTN 3	Oct 1990	Simulation of the tropical diurnal cycle in a climate model. D P Rowell
CRTN 4	Oct 1990	Low frequency variability of the oceans. C K Folland, A Colman, D E Parker and A Bevan
CRTN 5	Dec 1990	A comparison of 11-level General Circulation Model Simulations with observations in the East Sahel. K Maskell
CRTN 6	Dec 1990	Climate Change Prediction. J F B Mitchell and Qing-cun Zeng
CRTN 7	Jan 1991	Deforestation of Amazonia - modelling the effects of albedo change. M F Mylne and P R Rowntree
CRTN 8	Jan 1991	The role of observations in climate prediction and research. D J Carson
CRTN 9	Mar 1991	The greenhouse effect and its likely consequences for climate change. D J Carson
CRTN 10	Apr 1991	Use of wind stresses from operational N.W.P. models to force an O.G.C.M. of the Indian Ocean. D J Carrington